Bat swarming as an inspiration for multi-agent systems: predation success, active sensing, and collision avoidance

Yuan Lin

Dissertation submitted to the Faculty of the
Virginia Polytechnic Institute and State University
in partial fulfillment of the requirements for the degree of

Doctor of Philosophy
in
Engineering Mechanics

Nicole T. Abaid, Co-chair
Rolf Müller, Co-chair
H. Pat Artis
Mark S. Cramer
Shane D. Ross

February 1, 2016
Blacksburg, Virginia

Keywords: Bat Swarming, Predation Success, Frequency Jamming, Collision Avoidance, Swarm Size

Bat swarming as an inspiration for multi-agent systems: predation success, active sensing, and collision avoidance

Yuan Lin

Abstract

Many species of bats primarily use echolocation, a type of active sensing wherein bats emit ultrasonic pulses and listen to echoes, for guidance and navigation. Swarms of such bats are a unique type of multi-agent systems that feature bats echolocation and flight behaviors. In the work of this dissertation, we used bat swarming as an inspiration for multi-agent systems to study various topics which include predation success, active sensing, and collision avoidance. To investigate the predation success, we modeled a group of bats hunting a number of collectively behaving prey. The modeling results demonstrated the benefit of localized grouping of prey in avoiding predation by bats. In the topics regarding active sensing and collision avoidance, we studied individual behavior in swarms as bats could potentially benefit from information sharing while suffering from frequency jamming, i.e., bats having difficulty in distinguishing between self and peers information. We conducted field experiments in a cave and found that individual bat increased biosonar output as swarm size increased. The experimental finding indicated that individual bat acquired more sensory information in larger swarms even though there could be frequency jamming risk. In a simulation wherein we modeled bats flying through a tunnel, we showed the increasing collision risk in larger swarms for bats either sharing information or flying independently. Thus, we hypothesized that individual bat increased pulse emissions for more sensory information for collision avoidance while possibly taking advantage of information sharing and coping with frequency jamming during swarming.

The research is supported by the National Science Foundation [grant CMMI-1342176], the National Natural Science Foundation of China [grant numbers 10774092 and 451069], the Chinese Ministry of Education (Tese Grant), the Institute for Critical Technology and Applied Science at Virginia Tech, and the Fundamental Research Fund of Shandong University [No. 2014QY008].

Acknowledgments

I would like to thank all the people who have been supportive to me pursuing my doctoral degree at Virginia Tech. First of all, I would like to thank both my advisors, Drs. Abaid and Müller, for their tremendous help during my research years. Dr. Abaid brought me to the field of multi-agent systems and advised me to learn the method of agent-based modeling. My MATLAB coding skill was also improved under her advisorship. Since I joined Dr. Müller's lab in Fall 2014, I obtained better knowledge in biosonar systems and signal processing. Dr. Müller also offered me critical advice that improved my scientific writing. I also wouldn't forget that Dr. Müller gave me a hand when I had trouble in graduate school.

The other three committee members were also helpful in my doctoral study in many aspects. I enjoyed my interactions with Dr. Artis, who was always helpful in me pursuing my career. Dr. Artis gave me comments on my writing and offered me advice to help me succeed. Dr. Cramer was helpful in me learning engineering mechanics courses, which had me think about problems and issues from a totally different perspective. I enjoyed taking the courses in dynamical systems and control by Dr. Ross. Dr. Ross explained dynamics topics in very clear ways, which benefited me a lot in my logical thinking.

I was also grateful to having taken the robotics courses and worked with Dr. Kevin Kochersberger on unmanned systems at Virginia Tech. I developed great interest in robotics through the projects that I did on unmanned ground/aerial vehicles. Particularly, I had the opportunity to work with Dr. Kochersberger on drone application in farming in his Unmanned Systems Lab, where I saw the possibility of immediate use of university technology in the real world.

There are so many people who encouraged me so much at whatever phases of my life. My mother is always proud of me; my father loves me with few words; my sister shares with me articles with deep societal and historical meanings. Jay and Michelle Lester and other attendees from International Christian Fellowship offered so much positive thinking

that turned me into a person with greater gratitude. My international group at New Life Christian Fellowship helped me through the alone years in the United States. There were so many friends (students, staff, and faculty) in the Engineering Mechanics program that provided invaluable help for me to pass the program exams to graduate.

In addition, I was blessed to have worked with other fellow hokies to start the Aerial Robotics Club (ARC) at Virginia Tech. The startup provided me opportunities to learn to lead a team in the United States and pursue my career in robotics with the help from multi-nationals. It was great to work with many amazing people from the club who are doing amazing things that could possibly change people's life.

Last but not least, I would like to express my gratitude to the Department of Biomedical Engineering & Mechanics and the Department of Physics at Virginia Tech as they hired me as a teaching assistant in the past years.

Contents

List of Figures

List of Tables

Chapter 1

Introduction

1.1 Multi-agent animal systems

Multi-agent systems are known as systems that include multiple autonomous agents in a environment [1]. Multi-agent systems are observed in various settings such as robotic teams [2, 3], computer networks [4], economic systems [5], and animal groups [6]. To our interest, we study multi-agent systems of animal groups, i.e., *multi-agent animal systems*, by taking animal swarming as an inspiration for multi-agent systems of broader sense.

Multi-agent animal systems usually involve interacting animals swarming in groups which can be characterized as collective behavior. Animals across different species show collective grouping, such as schooling fish [7], flocking birds [8], lane-forming ants [9], and column-forming bats [10]. It has been demonstrated that appropriate interaction rules among agents lead to collective formation (coherent moving direction and relatively close distance) [11]. The possible interaction rules may include alignment of velocity directions, attraction to peers' locations, and repulsion from peers that may cause collisions [12, 13].

While multi-agent swarming emerge due to the local interacting rules, the collective swarming also affects individual behavior reversely. The reverse relationship is characterized as group-size effect wherein swarm size correlates with individual behavioral change. For examples, individual bird vigilance reduces in larger groups due to collective detection and lower individual predation risk [14, 15]; wasp behavior is less complex in larger swarms for completing fewer tasks [16]; dairy cattle's food intake varies with group size because of feeding competition and social comfort [17]. These examples indicate that swarming results in both benefits and disadvantages for which animals modify individual behavior

to accommodate.

1.2 Bat swarms

Bat swarms are unique multi-agent animal systems due to the nature of bat echolocation. Echolocation is defined as bats emit ultrasonic pulses and listen to the reflected echoes for guidance and navigation [18, 19]. Thus, echolocation is a kind of active sensing [20, 21, 22] which is different from passive sensing wherein agents do not emit self signals but instead use only existing environmental information for sensing. Bats' acting sensing may post both constructive and destructive influences to individuals when bats form swarms. The influence is constructive if a bat possibly utilizes peers' sensory information/listen to peers' echoes for navigation, which is shown as bats' eavesdropping behavior [23, 24]. This is also known as information sharing in engineering systems [25]. On the other hand, the influence is destructive if a bat cannot distinguish self and peers' echoes for accurate navigation. This destructive influence is characterized as frequency jamming problem in bat groups [26, 27, 28]. To unveil bats' behavior in maximizing the constructive influence while minimizing the destructive influence during collision-free swarming is one of the research goals in this dissection, as the findings could potentially inspire novel control algorithms for next-generation unmanned aerial vehicles with decentralized control [2, 3].

1.3 Research topics and attribution

The research in the dissertation is focused on bat swarming while covering various topics which include hunting success, active sensing, and collision avoidance. The papers documenting the research results have been published in or will be submitted to various journals and are shown in the following chapters.

Specifically, for the topic of hunting success, we investigated the impact of prey collective formation extent on the predation success of a group of independent bats. We used the method of agent-based modelling and illustrated our findings through simulation results. Our results could potentially provide insights on the strategies for predation avoidance in multi-agent systems. The paper for this work (Chapter 2) has been published in the journal of Physical Review E [29]. A conference paper that documented the early stage of the results was published in the 2013 ASME Dynamics and Control Conference [30].

For the topics of active sensing and collision avoidance, we quantified the relationship be-

tween individual biosonar output and swarm size through field experiments. The research was conducted in a cave wherein we recorded bat swarms using a camera and an ultrasonic recorder. The results could help us understand the individual bat behavior for frequency jamming avoidance through a global finding. The paper for this work (Chapter 3) will be submitted to a journal [31].

At last, we studied the benefit of changing individual biosonar output with swarm size in a multi-agent system through simulation. We allowed bats to utilize peers' information in the model. The benefit was quantified as collision avoidance success as collision is one of the major concerns of real flights. This work could explain the findings through field experiments in Chapter 3. The paper for this work (Chapter 4) has been published in the Journal of Theoretical Biology [32]. A conference paper that documented the early stage of the results was published in the 2014 ASME Dynamics and Control Conference [33].

Chapter 2

Bat predation success and prey collective behavior - simulation

This chapter has been published in Physical Review E with the title “Collective behavior and predation success in a predator-prey model inspired by hunting bats” [29].

2.1 Abstract

We establish an agent-based model to study the impact of prey behavior on the hunting success of predators. The predators and prey are modeled as self-propelled particles moving in a three-dimensional domain and subject to specific sensing abilities and behavioral rules inspired by bat hunting. The predators randomly search for prey. The prey either align velocity directions with peers, defined as “interacting” prey, or swarm “independently” of peer presence; both types of prey are subject to additive noise. In a simulation study, we find that interacting prey using low noise have the maximum predation avoidance because they form localized large groups, while they suffer high predation as noise increases due to the formation of broadly dispersed small groups. Independent prey, that are likely to be uniformly distributed in the domain, have higher predation risk under a low noise regime as they traverse larger spatial extents. These effects are enhanced in large prey populations, which exhibit more ordered collective behavior or more uniform spatial distribution as they are interacting or independent, respectively.

2.2 Introduction

Collective behavior is a striking phenomenon observed in animals of diverse species, like fish swimming in schools [7], birds flying in flocks [8], ants forming organized lanes [9], and mosquitoes flying in swarms [34]. This social behavior is known to provide a variety of benefits for individuals. For example, it may increase the chance for animals to locate food sources [35], conserve heat and energy of a colony [36], help an individual find a mate [37], and reduce the risk of being predated [38]. The benefit of protection from predation, which is of primary interest in this paper, results from the "many eyes" effect [15] and cognitive fusion to predators [39] when animals swarm in groups. The "many eyes" effect enables individuals to have better predator detection through information sharing with peers. An individual's risk of being attacked is diluted by the presence of other group members, which may coalesce into a superorganism in the predator's perception.

Capturing the dynamics of such groups is of interest to a variety of scientific and engineering research questions. In the literature, collective behavior is modeled either through continuum approaches or by establishing agent-based models. For one type of continuum approach, the Navier-Stokes equations are applied to study collective behavior as the motion of a fluid [40, 41]; for another continuum-type approach, equations are derived using self-propulsion and velocity reorientation of particles obeying a discrete model [42]. In addition to these modeling efforts, extensive research has been devoted to developing agent-based models, wherein individuals are considered as dynamic particles interacting with peers homogeneously [43]. The agent's behavioral responses are defined using discrete decision making [44, 45] or by building potential functions based on the state of the group [46, 47, 48]. Among models defining a decision making process, common rules applied to individuals for interacting with peers include "repulsion", "alignment", and "attraction". The "repulsion" rule mandates that each individual keeps a certain distance from peers; the "alignment" and "attraction" rules dictate that group members seek consensus in orientations and positions, respectively. Typical models based on such rules and potential functions generate collective behavior [12, 13, 49, 34] as group-level structures emerge from established principles of behavioral algorithms prescribed to individuals [11].

Research using agent-based models has also tackled the predator-prey relationship; such work finds that the relative population sizes, as well as overall species fitness, can be refined by varying model parameters. In [50], the ranges of sensing for predators and prey are varied to explore a model with carnivorous predators, herbivorous prey, and plants subject to behavioral rules. The authors find that increasing the sensing range for predators is beneficial for individual survival and detrimental for predator population size; analogously, increasing prey sensing range results in a smaller prey population. The steady-state pop-

ulation dynamics of predators and prey are investigated in [51], which finds that agents' initial conditions and the spatial arrangement and availability of resources for prey, such as food and refuge, determine the distribution of system behaviors. We comment that these studies only consider agents moving in discrete two-dimensional domains.

In this paper, we establish an agent-based predator-prey model in a three-dimensional domain to explore the relationship between the collective behavior of prey and predation success. The agents, predators and prey, are modeled as self-propelled particles inspired by rules common to the animal kingdom, that is, both predators and prey sense the environment, and predators hunt for and feed on prey. In the model, the sensing mechanisms and behavioral rules implemented in predators and prey represent the biological system of insectivorous bats and the insects they hunt [52, 53, 54]. In particular, predators are equipped with a limited sensing space that is analogous to bats' sonar beam pattern [55, 56], which is a key factor in determining their hunting success, and the prey are not capable of sensing the predators. We consider two cases in terms of prey's behavior: i) prey exhibit collective behavior à la Vicsek [57] by orienting velocity directions with peers subject to additive noise, and ii) prey swarm independently as random walkers subject to noise. By comparing simulation results of the two prey-swarming cases, we find that, in a sufficiently large environment, prey forming a few localized cohesive groups have a low chance of being detected by predators. Conversely, if prey are uniformly positioned in the environment, limited rather than extensive traversal of the domain is a better strategy to avoid predation. These results validate the current views held in the biological community that protection from predation is a significant motivator of collective behavior.

2.3 Modeling

2.3.1 Model description

We consider a system of $\hat{N} + N$ agents moving in a cube of side length L with periodic boundary conditions in discrete time. In the three-dimensional domain, the agents are partitioned into $\hat{N}$ predators and N prey with constant velocity magnitudes $\hat{s}$ and s, respectively. Each predator has a three-dimensional sensing space, a spherical cone. For the spherical cone, its apex is the predator's position; its side length is the predator's sensing range $\hat{r}_s$; and its opening angle is the predator's angular range of sensing $\hat{\phi}$. The predator's velocity vector starts at the apex of the spherical cone and aligns with its central axis. For

predator i, $i = 1, 2, \ldots, \hat{N}$, the position update at time $t + \Delta t$ is

$$\hat{\mathbf{x}}_i(t + \Delta t) = \hat{\mathbf{x}}_i(t) + \hat{\mathbf{v}}_i(t + \Delta t)\,\Delta t \tag{2.1}$$

where t, $\Delta t \in \mathbb{R}^+$, Δt is a constant, and $\hat{\mathbf{x}}_i$, $\hat{\mathbf{v}}_i \in \mathbb{R}^3$ are the predator's position and velocity vectors, respectively.

Each prey has a spherical sensing space whose center is the prey's position and whose radius equals the prey's sensing range r_s. At time t, the position vector of prey k, $k = 1, 2, \ldots, N$, is $\mathbf{x}_k(t) \in \mathbb{R}^3$ and its velocity vector is $\mathbf{v}_k(t) \in \mathbb{R}^3$. The position update for prey is the same as above for predators in (2.1). A schematic of the model geometry is shown in Figure 2.1.

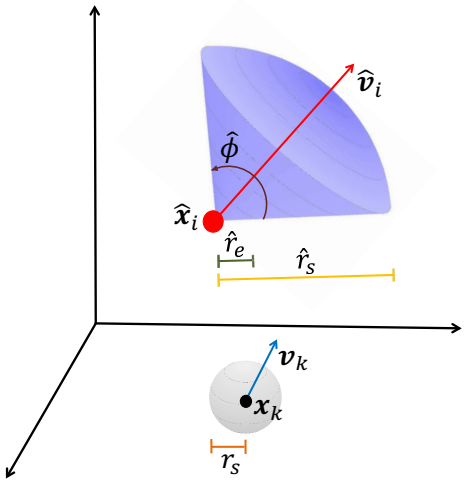

Figure 2.1: Schematic of three-dimensional sensing geometry for one predator (red circle) and one prey (black circle). The predator i has position $\hat{\mathbf{x}}_i$ and velocity $\hat{\mathbf{v}}_i$; the prey k has position $\mathbf{x}_k$ and velocity $\mathbf{v}_k$. The blue cone shows the predator's sensing space with sensing range $\hat{r}_s$, angular range $\hat{\phi}$, and eating range $\hat{r}_e$. The grey sphere shows the prey's sensing space with sensing range r_s.

The initial positions and velocity directions of predators and prey in $\mathbb{R}^3$ are generated with uniformly distributed random probability in the cube of side length L centered at the coordinate origin and in the unit sphere [58], respectively. The state update for both predators and prey depends only on the preceding time step. In the following, we define algorithms to update the velocity directions of predators and prey.

2.3.2 Predator velocity update algorithm

In the model, predators are designed to randomly search in the domain until they detect prey, after which they head towards the nearest prey detected. Thus, we define the following two rules to update the velocity directions for predators: a predator heads towards ("hunts") prey if prey are detected and walks randomly if prey are not detected.

The hunting rule mandates that predators head towards prey that occupy their sensing spaces. When a predator's sensing space is occupied by at least one prey, the predator chooses the nearest prey as a target and orients its velocity direction towards it persistently until the prey is no longer in the sensing space, which is similar to hunting in big brown bats [59]. If the distance between the predator and the prey is less than the eating range $\hat{r}_e$ in the sensing space, the prey is considered to be "eaten". In this case, the prey's position and velocity vectors are randomly reassigned with uniform distribution at the next time step, which results in a prey population of fixed size. When the hunted prey is eaten, the predator chooses the next closest prey in its sensing space and keeps on hunting. We comment that prey that are isolated are not preferentially selected as targets of predators, since the periodic boundary conditions constrain the prey population by design. We define the set of prey that occupy predator i's sensing space at time t as $\mathcal{N}_i(t)$ and the index of the prey targeted as k^*. Then the hunting velocity update for the predator is

$$\hat{\mathbf{v}}_i^h(t+\Delta t) = \hat{s}\,\frac{\mathbf{x}_{k^*}(t)-\hat{\mathbf{x}}_i(t)}{\|\mathbf{x}_{k^*}(t)-\hat{\mathbf{x}}_i(t)\|},\ k^*\in\mathcal{N}_i(t) \tag{2.2}$$

If there are no prey in a predator's sensing space, the predator behaves as an independent random walker. In this case, a predator's velocity direction relies only on its previous velocity perturbed by a random noise defined by a perturbation parameter $\hat{\eta}$. The random-walking velocity update for the predator is

$$\hat{\mathbf{v}}_i^w(t+\Delta t) = \hat{s}\,\frac{\hat{\mathbf{v}}_i(t)+\boldsymbol{\omega}(\hat{\eta})}{\|\hat{\mathbf{v}}_i(t)+\boldsymbol{\omega}(\hat{\eta})\|} \tag{2.3}$$

where $\boldsymbol{\omega}(\hat{\eta})\in\mathbb{R}^3$ is a realization of a vector-valued random variable whose magnitude is given by a Gaussian distribution with mean zero and standard deviation $\hat{s}\tan(\hat{\eta}\pi)$ and whose direction is uniformly distributed in the plane that is normal to the predator's velocity direction at time t. The magnitude of $\boldsymbol{\omega}(\hat{\eta})$ is restricted to the interval $[0,\hat{s}\tan(\hat{\eta}\pi)]$, which enforces the angle between $\hat{\mathbf{v}}_i^w(t+\Delta t)$ and $\hat{\mathbf{v}}_i(t)$ is less than or equal to $\hat{\eta}\pi$. When $\hat{\eta}=0$, the angle between these two vectors is always zero; when $\hat{\eta}=1$, this angle varies between zero and π. Loosely speaking, larger values of $\hat{\eta}$ result in higher random noise added at each time step, and thus, more convoluted trajectories for the predators. To avoid

unrealistically large values of this noise, which may occur since the Gaussian distribution is defined in $\mathbb{R}$, the realization of the random variable is regenerated when its magnitude has a value outside the stated interval. This restriction also ensures that the normalization with respect to the random noise term is defined.

We update the predator's velocity using the hunting and random-walking updates as

$$\hat{\mathbf{v}}_i(t+\Delta t) = \begin{cases} \hat{\mathbf{v}}_i^h(t+\Delta t), \text{ for } \mathcal{N}_i(t) \neq \emptyset \\ \hat{\mathbf{v}}_i^w(t+\Delta t), \text{ else} \end{cases}$$

We note that predators in the model do not interact with their peers, which is selected to agree with observations on groups of bats that congregate socially but do not move or hunt as a typical collective [60].

2.3.3 Prey velocity update algorithm

Based on whether or not prey interact with each other, we define two types of prey behavior to update their velocity directions: interacting prey align velocity directions with peers with Gaussian-distributed random noise and independent prey swarm randomly in addition to noise.

The alignment ability is defined for interacting prey in three dimensions based on Vicsek's model [61]. If the distance between a prey's position and its peer's position is less than the prey's sensing range r_s, the peer occupies the prey's sensing space. We denote $\mathcal{N}_k(t)$ as the set of indices of prey that occupy prey k's sensing space at time t, with $k \in \mathcal{N}_k(t)$ by convention. Prey k's provisional velocity update, $\mathbf{u}_k(t+\Delta t)$, is given by the average of the velocity vectors of prey $l \in \mathcal{N}_k(t)$. In other words,

$$\mathbf{u}_k(t+\Delta t) = s\,\frac{\sum_{l\in\mathcal{N}_k(t)} \mathbf{v}_l(t)}{\|\sum_{l\in\mathcal{N}_k(t)} \mathbf{v}_l(t)\|} \tag{2.4}$$

The provisional velocity update is perturbed by Gaussian-distributed random noise defined by a perturbation parameter η, which is analogous to random walking for predators defined above. Therefore, we obtain the velocity update for prey k as

$$\mathbf{v}_k(t+\Delta t) = s\,\frac{\mathbf{u}_k(t+\Delta t) + \boldsymbol{\omega}(\eta)}{\|\mathbf{u}_k(t+\Delta t) + \boldsymbol{\omega}(\eta)\|} \tag{2.5}$$

Independent prey swarm randomly using a rule analogous to the random walking velocity update in predators [62]. However, independent prey use the noise parameter η similarly

to interacting prey. The two types of prey behavior can be achieved by using $r_s \neq 0$ for interacting prey and $r_s = 0$ for independent prey. In other words,

$$\mathbf{u}_k(t + \Delta t) = \mathbf{v}_k(t) \tag{2.6}$$

for independent prey, since interactions with peers are not considered. With the maximum noise at $\eta = 1$, interactions among prey are totally dominated by noise and both interacting and independent prey exhibit the same random swarming behavior. We note that, although we define interactions among prey based on metric distances in line with [57, 61], similar collective behavior also results from prey interacting with peers selected using topological distances [7, 8], which may be implemented analogously.

We comment that prey's velocity update is not influenced by predators' behavior because prey do not detect predators in the model. As a result, there is no self-protection in prey from being predated upon. This assumption is in accordance with examples of insectivorous bats' prey, such as flying beetles, which do not evade hunting bats [63]. Moreover, lack of bi-directional perception between predators and prey necessitates the selection of only a single time scale for the decision making process, which is based on the predators alone since their hunting success is the variable of interest.

2.4 Observables

We define four observables to evaluate the behavior of prey: polarization, cohesion, cell occupancy parameter, and cell coverage. The polarization measures the alignment of prey; the cohesion captures prey grouping; the cell occupancy parameter conveys the spatial distribution of prey grouping; and the cell coverage shows the extent covered by an average prey trajectory. Note that high polarization, cohesion, and cell occupancy parameter values indicate prey collective behavior for moderate or large prey population sizes. Finally, the predation success is quantified as the average number of prey eaten by each predator per time step.

The polarization of prey is calculated as the absolute value of their average normalized velocities [57]. In other words, the prey polarization at time t is

$$p(t) = \frac{1}{N} \left\| \sum_{k=1}^{N} \frac{\mathbf{v}_k(t)}{s} \right\| \tag{2.7}$$

The value of $p(t)$ ranges from 0 to 1, where 0 means that prey velocity directions are homogeneously oriented in the unit sphere and 1 means that all prey are moving in the same direction. Note that, the polarization is 1 for the number of prey $N = 1$.

We compute the prey cohesion based on the method of average nearest neighbor [64], which allows equally high values when prey form large or small groups. In particular, the cohesion is given by the average distance between prey and their nearest peers [65]. With a reference distance L_d, the prey cohesion at time t is

$$c(t) = \exp\left(-\frac{1}{NL_d}\sum_{k=1}^{N} d_k(t)\right) \tag{2.8}$$

where

$$d_k(t) = \min_{l\neq k} \|\mathbf{x}_l(t) - \mathbf{x}_k(t)\|,\ l = 1, 2, \ldots, N \tag{2.9}$$

is the distance between prey k and its nearest peer at time t. The reference distance L_d is defined as the cut-off length between peers that are nominally near and far and thus can be used to tailor the absolute magnitude of cohesion. The cohesion $c(t)$ varies between 0 and 1, where a large value indicates high cohesion.

To obtain the cell occupancy parameter and cell coverage, we divide the cubic domain into cubic cells with equal side length L_c. We select L_c as a factor of L so that the number of cells is $(L/L_c)^3$, which is an integer. The number of prey in cell m, denoted as $n_o(m, t)$, divided by the total number of prey N is the normalized cell occupancy $o(m, t)$ of the cell at time t. In other words,

$$o(m, t) = \frac{n_o(m, t)}{N} \tag{2.10}$$

The normalized cell occupancies of all the cells are sorted by magnitude from greatest to least to obtain the normalized sorted cell occupancy at time t, which quantifies the extent of prey groups similarly to the density profiles considered in [66]. The distribution of the normalized sorted cell occupancy which shows large occupancy values for a small number of cells indicates that prey form a small number of large groups. On the contrary, flatter distributions show that prey individuals are likely to be uniformly distributed in the domain. Since most distributions exhibit approximately exponential decay based on inspection, we average the normalized sorted cell occupancy with respect to time for the simulation and fit it with an exponential probability density function [67], which is

$$f(y, \lambda) = \lambda e^{-\lambda y} \tag{2.11}$$

where y is the index of the average sorted cell occupancy for each cell, which is a positive integer between one and the total number of cells, f is the average normalized sorted cell occupancy, and λ is the cell occupancy parameter obtained by fitting the above distribution. The value of λ is larger for distributions which are peaked for a small number of cells and

Table 2.1: Parameter values for predators and prey.

	Predators		Prey		
Parameter	Symbol	Value	Symbol	Value	Unit
Population size	$\hat{N}$	10	N	5 - 1000	-
Speed	$\hat{s}$	0.5	s	0.25	$\mathrm{m}/\Delta\mathrm{t}$
		5		2.5	m/s
Sensing range	$\hat{r}_s$	5	r_s	2.5	m
Perturbation parameter	$\hat{\eta}$	0.1	η	0 - 1	-
Time interval for cell coverage	-	-	$\Delta\tau$	150	$\Delta\mathrm{t}$
Angular range of sensing	$\hat{\phi}$	120	-	-	$^\circ$
Eating range	$\hat{r}_e$	0.5	-	-	m
Reference distance for cohesion	-	-	L_d	5	m

exhibit fast decay, and it is smaller for distributions which are approximately constant and exhibit slow decay.

The discrete spatial cells are also used to measure the straightness of prey' paths. We define the cell coverage for prey k, denoted as $n_c(k,t)$, to be the number of distinct cells that the prey's trajectory occupies during the time interval $[t, t+\Delta\tau]$ for a constant $\Delta\tau \in \mathbb{R}^+$. Cell coverage with a value of one means that the prey resides in the same cell with a convoluted trajectory over the time interval, while a higher cell coverage value means that the prey traverses a large extent of the domain by moving over a fairly straight path. Note that, when computing the cell coverage for prey, we neglect time intervals in which prey are eaten because their positions are regenerated randomly in the domain which results in discontinuous prey trajectories.

The average number of prey eaten by each predator per time step is obtained to evaluate predation success during simulation. This quantity is calculated as

$$\bar{n}_e = \frac{N_e}{\hat{N}T} \tag{2.12}$$

where N_e denotes the total number of prey eaten over the entire simulation length in time steps, defined as T. We comment that this metric is normalized by the number of predators to highlight their ability to hunt in the environment of variable resources and is thus not normalized by the number of prey present.

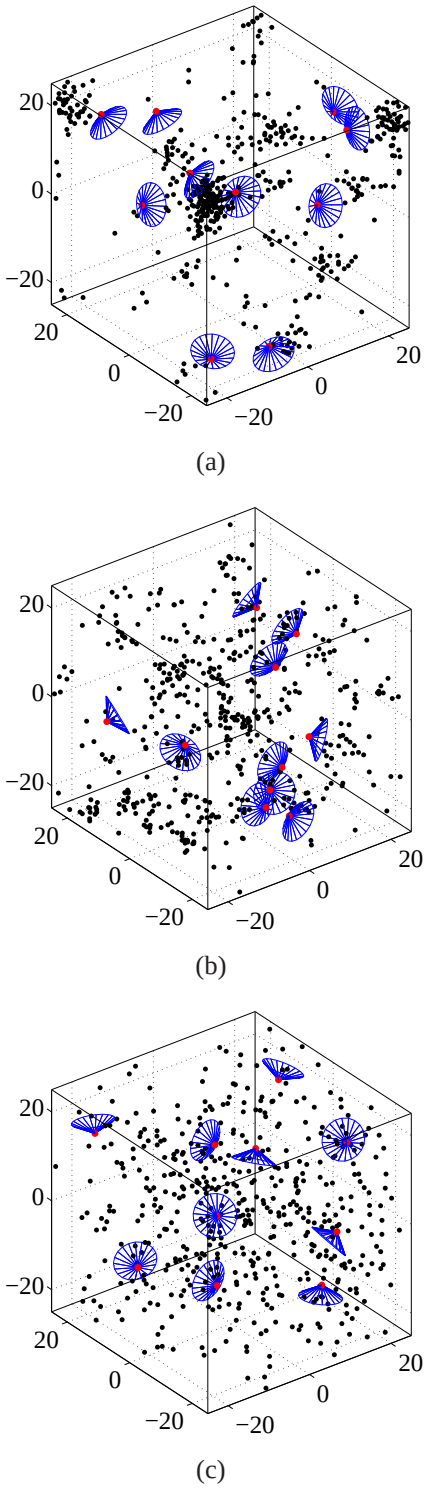

Figure 2.2: Frames of model simulation with 10 predators and 500 interacting prey when (a) $\eta = 0$, (b) $\eta = 0.2$, and (c) $\eta = 1$. Red dots show predators' positions which coincide with the apex of the blue spherical cones showing their sensing spaces; black dots show prey's positions. The unit for the numbers on the axes is meter.

2.5 Simulation results

We seek to determine the parameters of the model for the simulation study by taking inspiration from biological systems. The predators' sensing range is taken as $\hat{r}_s = 5\mathrm{m}$ and their angular range of sensing is $\hat{\phi} = 120°$, which are physical parameters from big brown bats, *Eptesicus fuscus* [59, 68]. The prey's sensing range is taken as half that of the predators', which is $r_s = 2.5\mathrm{m}$. The predator speed is taken as the bat nominal flying speed $5\mathrm{m/s}$ [69] and the same proportionality between predator and prey sensing ranges is assumed for their velocities. With the prey velocity smaller than the predators', the predators are likely to achieve predation once they sense prey. We consider the population size of predators as $\hat{N} = 10$ and the side length of the domain as $L = 50\mathrm{m}$, such that the density of predators is 0.08 per $1000\mathrm{m}^3$. The low density of predators in the domain ensures sufficiently large space for each predator to hunt and lowers their chance of collisions that are neglected in the model, consistently with collision avoidance in bats' behavior [54]. The perturbation parameter for the predator swarm is $\hat{\eta} = 0.1$, which results in relatively straight trajectories which may occur in bats' flights [70, 71].

We take the eating range $\hat{r}_e$ as the distance a predator travels in one time step which is defined as $\Delta t = 0.1\mathrm{s}$ for all simulations. In computing prey cohesion, we take the cut-off length $L_d = 5\mathrm{m}$ equal to the diameter of the prey spherical sensing space, which is the threshold above which two prey are not able to interact directly or indirectly through common neighbors. By this definition, two prey separated by L_d have a cohesion of $1/e = 0.368$, which defines a nominally small value for this observable. For the simulation study, we consider the hunting behavior of predators with various prey population sizes ranging from 5 to 1000. Thus, the density of prey varies from 0.04 per $1000\mathrm{m}^3$ to 8 per $1000\mathrm{m}^3$. The side length of the cubic cells is taken as $L_c = 10\mathrm{m}$, such that the volume of one cell is $1000\mathrm{m}^3$ and the total number of cells in the domain is 125. The time interval for prey cell coverage, $\Delta\tau$ is taken as 150 Δt, which gives $37.5\mathrm{m}$ if a prey travels straight with velocity of $0.25\mathrm{m}/\Delta t$. This selected time interval ensures that a prey can potentially traverse multiple cells, while eliminating double counting a periodic trajectory since the maximum distance that a prey travels is less than L. For both cases of interacting prey and independent prey, the prey perturbation parameter η varies from 0 to 1, which enables us to obtain both the minimum and maximum effects from random noise. Table 2.1 gives a summary of the parameter values used in the simulation study.

Figure 2.2 shows exemplary frames of predators and interacting prey swarming in simulations with $N = 500$. We see that, with $\eta = 0$, interacting prey form relatively large groups, while with $\eta = 0.2$, they form small groups comprising a few nearby peers. When $\eta = 1$, interacting prey are likely to be homogeneously positioned in the domain with

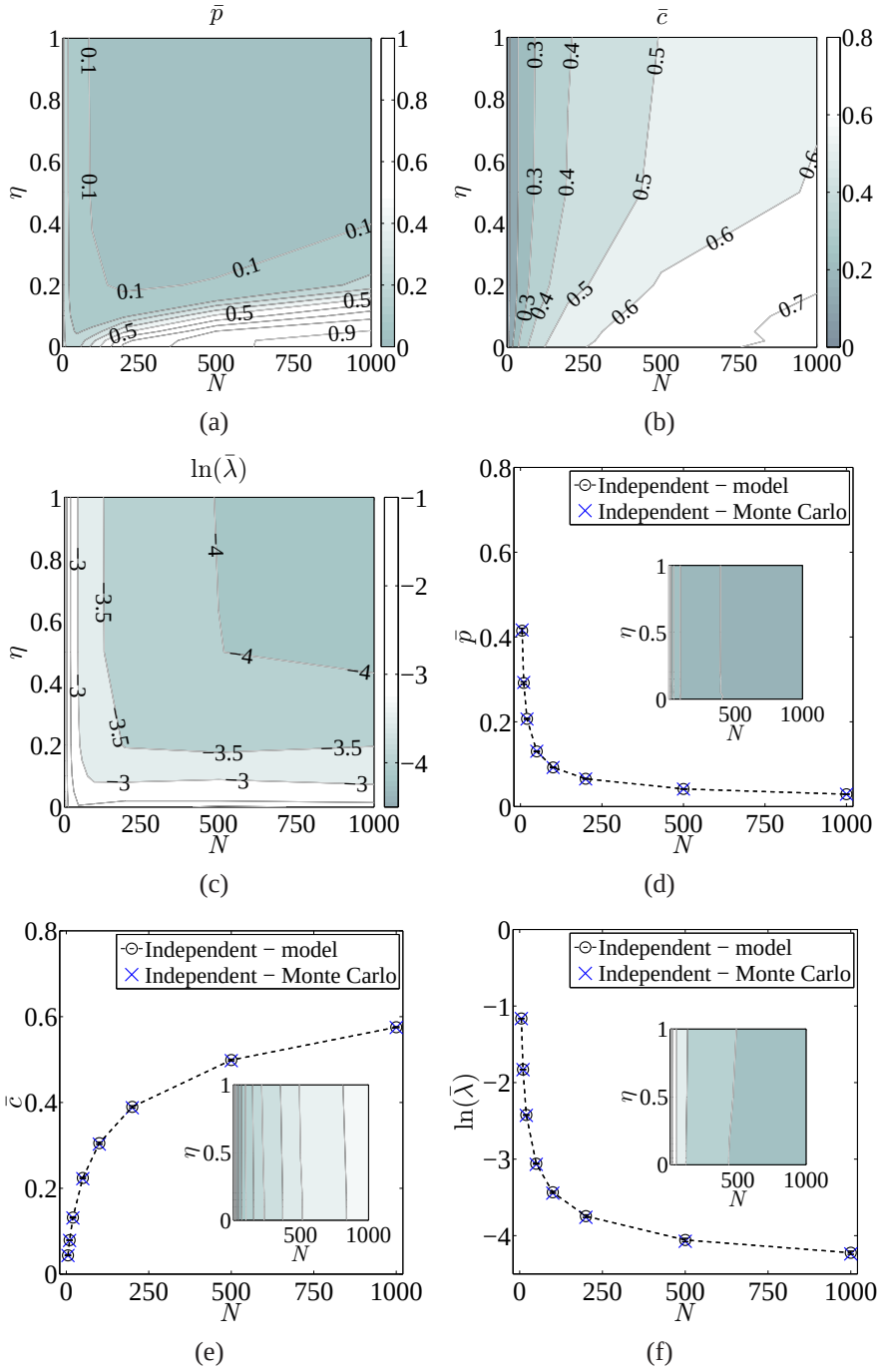

Figure 2.3: Mean ((a) and (d)) polarization, ((b) and (e)) cohesion, and ((c) and (f)) natural logarithm of cell occupancy parameter for interacting and independent prey, respectively. Contour plots are displayed as prey population size N and perturbation parameter η are varied. The black circles show the mean observable values obtained from the model with independent prey and the blue crosses show results of Monte Carlo simulations. The superscript bar notation denotes the mean over the replicates and the error bars denote standard deviations over all selected values of η. Insets in the second row show contour plots for independent prey. For each inset, the color map is consistent with the contour plot above, that is, with the corresponding observable for interacting prey.

no observable clusters. Thus, the three representative values of η - 0, 0.2, and 1 - are considered to be associated with low, moderate and high noise for prey, respectively. For simulations with independent prey, the distributions of particles in the domain are similar to Figure 2.2(c). In addition, the motion of each agent follows a straighter trajectory as the noise is decreased.

For the simulation study, we take $T = 25\,000$ time steps as one simulation replicate and average the prey's polarization, cohesion, normalized sorted cell occupancy, cell coverage, and the predator's predation success within each replicate with respect to time. Moreover, the cell occupancy parameter λ for each replicate is obtained by fitting the average normalized sorted cell occupancy to the exponential probability density function; the cell coverage values are obtained for each replicate by partitioning the time series into time intervals of length $\Delta\tau$. Simulations are recorded after excluding an initial transient phase of $10\,000$ time steps. Fifteen replicates are considered for each set of parameters. The number of replicates and the simulation length are selected to ensure stationarity of the results. In other words, the mean of the averages for the observables over the 15 replicates divided by their standard deviation is less than 10%.

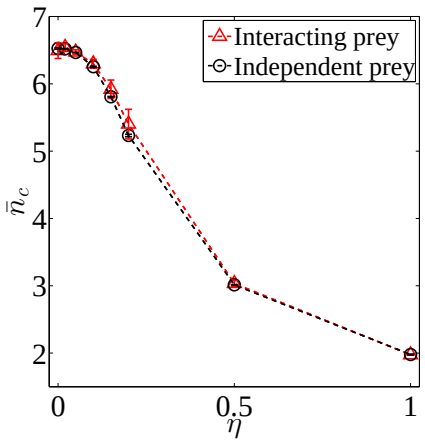

(a)

Figure 2.4: Mean prey cell coverage, as prey perturbation parameter η is varied. The superscript bar notation denotes the mean over the 15 replicates and the error bars denote standard deviations over all selected values of N.

Through observation, we find that the mean polarization, cohesion, and cell occupancy parameter λ values remain practically constant for independent prey of fixed population size as noise is varied; this result is absent for interacting prey. Thus, we report the polariza-

tion, cohesion, and cell occupancy parameter values for interacting prey in contour plots as the number of prey N and the prey perturbation parameter η are varied in Figure 2.3(a), Figure 2.3(b), and Figure 2.3(c), respectively. These quantities are shown for independent prey in plots with varying N only, see the black dashed curves in Figure 2.3(d), Figure 2.3(e), and Figure 2.3(f); insets inside these three plots display the contour plots which show vertical striation characteristic of the observables. We comment that many contours do not appear smooth due to the small number of data points for large prey population sizes and the lack of smoothing the raw data.

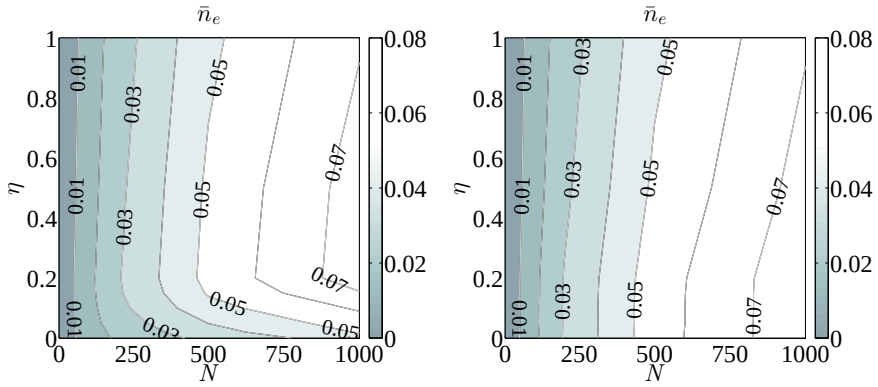

Figure 2.5: Mean number of eaten (a) interacting and (b) independent prey, as prey population size N and perturbation parameter η are varied.

The polarization, cohesion, and cell occupancy parameter values of independent prey are verified through a Monte Carlo simulation. We comment that the expected value for polarization may be computed analytically as a function of N in terms of random variables defining uniformly distributed points on the unit sphere [58]. However, this procedure requires evaluating $2N$ nested integrals, which poses both analytical and numerical challenges. Due to the nearest neighbor selection process inherent in the cohesion computation and the sorting of cell occupancies, the cohesion and cell occupancy parameter may not be analytically defined in integral expressions. Thus the Monte Carlo simulation is selected for comparison of these observables to the model simulation. In the Monte Carlo simulation, the particles are assigned with random velocity directions and positions at each time step, thus omitting the dynamics of the model. The Monte Carlo simulations are computed with 10 replicates analogously to the model simulations; observable values are also obtained in the same way as above. The quantities from the Monte Carlo simulation are denoted as blue crosses in the plots for independent prey.

In Figure 2.3(a), we see that the addition of noise is destructive to the polarization of interacting prey. When the noise is low, interacting prey are highly polarized. However, when the noise increases to the moderate level at $\eta = 0.2$, the polarization of interacting prey drops steeply to low values, which are practically constant as the noise increases to its maximum at $\eta = 1$. For a fixed value of noise, there is a non-monotonic trend accompanied with increasing population sizes for interacting prey: polarization decreases to a minimum value for a relatively small population size and increases as population size grows further. Figure 2.3(d) shows that the polarization of independent prey decreases with increasing prey population size for all values of noise, as evidenced by the small error bars.

In Figure 2.3(b), low noise results in higher cohesion in interacting prey of fixed moderate or large population sizes. This effect is absent in independent prey whose cohesion depends exclusively on N in Figure 2.3(e). Generally speaking, cohesion values increase with larger prey population sizes for both interacting and independent prey.

In Figure 2.3(c), we see that low noise corresponds to large values of the natural logarithm of the cell occupancy parameter, $\ln(\lambda)$, in interacting prey. Simulations with high noise have low $\ln(\lambda)$ values in interacting prey for moderate or large prey population sizes, similarly to independent prey with all levels of noise in Figure 2.3(f). Note that, due to the normalization of the sorted cell occupancy, the fitting gives large $\ln(\lambda)$ values for a small number of prey.

Curves, as opposed to contour plots, are also selected to show the cell coverage for both interacting and independent prey because its values for a fixed prey noise are found to be nearly constant for all prey population sizes N, see the small error bars in Figure 2.4. We see that increasing noise results in decreasing cell coverage for both types of prey, which means the prey's trajectories are less straight and cover fewer cells with high prey noise. We comment that the cell coverage for both interacting and independent prey are practically indentical, evidencing that random noise rather than the averaging protocol determines the cell coverage values.

The predation success for both interacting and independent prey is shown in contour plots in Figure 2.5, as its values vary with both N and η. In Figure 2.5(a), we see that interacting prey are least eaten with noise close to zero, while they suffer the highest predation with the moderate noise at $\eta = 0.2$; when noise increases from the moderate value, they have increased protection from predation. Figure 2.5(b) shows that increasing noise is universally positive to independent prey for avoiding predation. Moreover, all the above effects about predation success are enhanced with larger prey population sizes.

The relationship between the observables can be observed by computing the correlation coefficient R using a t-test [72]. The test statistic $t = \sqrt{(R^2(\nu - 2)/(1 - R^2))}$ where ν is

the degrees of freedom. We take $p < 0.05$ as significant. For polarization, cohesion, cell occupancy parameter, and predation success, the correlations are calculated between each pair of observables for all values of N and η considering both the prey population size and noise effects; the quantity ν is the product of the number of perturbation parameter values and the number of prey population sizes tested, which is $8 * 8 = 64$ in this case. We find that, for interacting prey, the cohesion and cell occupancy parameter are both significantly correlated with predation success (Cohesion: $R = 0.89$, $p < 0.01$. Cell occupancy parameter: $R = -0.69$, $p < 0.01$.) and with each other ($R = -0.67$, $p < 0.01$); on the other hand, the polarization is not correlated with predation success ($R = 0.19$, $p = 0.13$). We further investigate the correlation between cell coverage and predation success for all η values with a fixed N, because cell coverage varies only with noise as seen in Figure 2.4; ν equals 8, the number of perturbation parameter values, in this case. Computing the correlation between cell coverage and predation success for each N of independent prey, we obtain the range of R values $[0.94, 0.97]$ with all $p < 0.01$, which means that cell coverage is significantly correlated to predation success for any prey population size for independent prey.

2.6 Discussion

Based on the simulation study with varying noise, interaction scheme, and prey population size, we find the following principles regarding predation avoidance: (i) when random noise is sufficiently low, interacting with peers is highly beneficial to avoid predation; (ii) for a prey population of fixed size, there is a maximum probability for interacting prey to be eaten when they use noise of a moderate value; and (iii) increasing noise increases the probability to avoid predation for independent prey, an effect which also exists in the case of interacting prey using high noise. Furthermore, these effects are enhanced by increasing the prey population size.

The benefit of protection from predation for interacting prey using low noise results from the formation of large and cohesive groups. For interacting prey, the alignment rule that prey orient velocity directions with peers results in coherent motion of prey as shown by the high polarization values for $\eta < 0.2$, consistent with previously published results [57]. The polarized collective motion induces cohesive prey groups, which confirms the observation in [7] that high polarization corresponds to high cohesion with a similar one-dimensional model. Noise added to the prey's orientation update has a destructive influence on the prey's collective behavior, which is seen by a steep reduction in polarization and cohesion. Further observation through the cell occupancy parameter values for inter-

acting prey shows that lower noise leads to the formation of larger groups. Larger groups result since, with less perturbation to the interaction from noise, prey are more likely to form groups and their coordinated motion is more stable. For sufficiently large prey population sizes, prey coalescing in a few large groups require the predators to search widely for them, which reduces their probability of being detected and predated. This finding is supported by the negative correlation between cell occupancy parameter values and predation success. Furthermore, this result agrees with the biological literature that cites protection from predation as a primary benefit of collective behavior [73, 74]. We comment that, due to its limited sensing space, a predator has low possibility to prey upon sufficiently large prey groups in their entirety, since not all group members are likely to successively occupy its sensing space. This prevents unfettered consumption of large prey populations by predators in the model and thus supports the benefit of forming large groups.

For an interacting prey population of constant size, there is a maximum probability of being predated when the prey form a number of small groups using moderate noise. At the moderate noise level occurring at approximately $\eta = 0.2$, the alignment of interacting prey is perturbed significantly and the prey form small groups compared to the case of low noise, as seen in the cell occupancy parameter values. These small groups occur in relatively large numbers and may move independently in the domain, which corresponds to the sharp decline in polarization. This is supported by the fact the cohesion reduces less as noise increases, as it is measured in terms of average nearest neighbors. The relatively large number of small groups are likely to be uniformly distributed in the domain, which increases their probability of being detected and predated by predators. In addition, if prey in a small group are detected by a predator, the predator may eat a large portion of the group in contrast to the previously mentioned case of large prey groups. Finally, these trends are supported by the positive correlation between prey cohesion and predation success.

Noise reduces the risk of being detected, and therefore predated upon, when prey swarm independently because high noise results in trajectories with less cell coverage. Independent prey have uniform spatial distribution in the domain, which means that a predator is near prey regardless of its position. When the noise is low, prey's trajectories are likely to be straight. In contrast, when noise is high, the prey's velocity directions are perturbed at every time step, which results in convoluted trajectories that are likely to cover fewer cells. Since prey are less likely to encounter predators that they are not initially near to when their trajectories cover fewer cells, prey using high noise are less likely to be detected and predated upon as a result. The reasoning is supported by the positive correlation between cell coverage and predation success for independent prey. This effect is also evident in interacting prey with noise that is sufficiently high to promote the group's uniform spatial

distribution in the domain.

The above effects are all enhanced by larger prey population sizes. For independent prey, the high density of prey in the domain increases the possibility of an individual to encounter predators and get eaten, as prey are likely to be uniformly distributed in the domain. For small interacting prey population sizes, the impact of interacting on the predation success is not obvious since prey's collective behavior fails to emerge for most noise levels. The sensing space of prey occupies only 0.01571% of the domain volume in the model. Therefore, prey with low density have low chance to interact with peers and do not exhibit emergent collective behavior, as evidenced by the non-monotonic trend in polarization with minimum values at small prey population sizes. The collective behavior is further hindered as prey are repeatedly eaten and random velocity and position vectors are reassigned for them. This fact can be seen by comparing the polarization values for interacting prey in the presence of predators to the simulations of the Vicsek model in three dimensions in [61], whose values are larger in magnitude. We note that when the number of prey is small, the polarization may be high because a limited number of prey velocity vectors have orientations which are more likely to be inhomogeneously distributed in the unit sphere. This size effect is demonstrated by the non-zero polarization of independent prey computed with both the model and Monte Carlo simulations, which vanishes with increasing group size.

In conclusion, coalescing in localized cohesive groups is an effective strategy for individuals to avoid predation by independent predators. For independent individuals, minimizing the straightness of path results in decreased predation as opposed to traversing large proportions of the domain, since traveling may expose their positions to predators and increase the risk of being detected. This modeling framework may be translated to diverse applications for studying the dynamics and control of multi-agent systems such as animal groups and robotic teams. Similar modeling strategies have been used to model characteristic circular motion in groups of planktonic crustaceans, *Daphnia* [75] and to control teams of robots locating static targets [76].

Future work will include generalizing the model to incorporate more diverse sensing schemes for predators, enabling them to sense and interact with each other [77, 78], as is observed in a variety of natural settings [79, 80, 81]. Potential emergence in the group of predators will broaden this work to allow exploring the role of collective behavior in aiding rather than hindering predation. Moreover, prey will be enabled to detect and evade predators [14, 82], which is expected to reduce the predation in the simulation and be more relevant to biological systems. The future work is anticipated to find applications in the area of biologically-inspired control of robot teams interacting with animal groups [83] or cooperating in dynamic, real-world environments [84, 85].

Chapter 3

Bat pulse emission and swarm size - field experiment

This chapter will be submitted to a journal for publication [31].

3.1 Abstract

Flying in swarms, e.g., when exiting a cave, could pose a problem to bats that use an active biosonar system because the animals could risk jamming each other's biosonar signals. Hypotheses derived from lab experiments or observations of pairs of bats in the field have suggested that bats may reduce jamming by shifting their frequency bands apart or by reducing the rate of their pulse emissions. In the present work, the number of Eastern bent-wing bats (*Miniopterus fuliginosus*) that were flying on the inside of a cave entrance during evening emergence was estimated along with the total number of biosonar pulses they produced. Over the range of bat numbers present in the analyzed recordings (0 to 15 bats), the estimate for the number of biosonar pulses per bat increased with the estimated number of bats present. No change in the type of pulses was observed and the discernible signals conformed with the characteristics of biosonar pulses. This can be interpreted as an indication that Eastern bent-wing bats flying increase their sonar pulse rates with the number of bats surrounding them in a swarm. This behavior could be explained by the hypothesis that the animals did not suffer from substantial jamming probabilities under the density regimes observed here, so jamming may not have been a limiting factor for their biosonar behavior. At the same time, the increasing numbers of bat present could

have posed a navigation challenge that could have been addressed by the higher pulse emission rates.

3.2 Introduction

Bats are a group of unique flying animals that use echolocation as their primary far-sense for guidance and navigation [69]. To accomplish this, they emit directional ultrasonic pulses [86, 55] and receive echoes reflected from the environment. At the same time, many bat species are highly social animals that roost in colonies formed by tens to thousands of individuals in caves [87, 88] or in buildings [89]. They swarm during cave emergence and open-field flight with the spatial formation being a column [90, 87]. Bat swarms can move in large densities at high speeds without fatal collisions with each other or objects in their environments [90, 10].

Swarming may pose unique challenges to bats since the operation of bat biosonar is usually understood as comparing an emitted pulse to an echo that was triggered by this pulse. For example, bats could estimate the distance to a target by measuring the delay between pulse and echo [91, 92] or gain information about the identity [18] or the elevation [93] of a target from spectral changes introduced into the pulse spectrum by the target's transfer function [94, 95]. In dense swarms, bats may have difficulty extracting individual echoes and matching them to their pulses. In other words, bats may suffer from frequency jamming due to the presence of peers' ultrasound [96, 28, 27].

It has been demonstrated that bats modify individual pulse emission behavior to cope with frequency jamming. In laboratory experiments with pairs of big brown bats (*Eptesicus fuscus*), it has been found that the bat ceased vocalization when following a peer [24]. Similarly, Mexican free-tailed bats (*Tadarida brasiliensis*) reduced individual emission rate with group size when kept stationary in a small cage [97]. Bats belonging several species have been observed to shift their ultrasound frequency bands during encounters with conspecifics, presumably to reduce spectral overlap and the probability of jamming [96, 28]. However, the contrary has also be observed. Taiwanese leaf-nosed bats (*Hipposideros terasensis*) were found to gradually reduce the differences in their ultrasound frequency bands in a laboratory colony [98]. There is currently no literature, however, documenting bat individual behavioral change in pulse emission in large swarms during flight and/or in the wild.

This work presented here has investigated whether bats adjust their biosonar output with swarm size in the field to better understand how bats may respond to the jamming risks

posed by flying in swarms. To this end, we have obtained recording of bats flying in a cave and their ultrasonic emission. We quantitatively studied bats' pulse emission as their swarm size increased. This work allowed us to test the current hypothesis in the literature that individual bat reduces pulse emission in the presence of peers. It also facilitated exploring new perspectives of bat pulse emission behavior under the complex goals of group flight which include both collision and jamming avoidance [99, 100].

3.3 Materials and methods

3.3.1 Animals and location

The field work was conducted in a limestone cave located in Wuyan County, Jiangxi Province, China (29°23.286'N, 117°42.125'E). The major portion of the cave had an approximately rectangular cross section with 1.75 m in width and 3 m in height, and had a total length of 9 m. The cave tilted slightly downwards in the direction away from the entrance. By observation, it was established that the cave housed at least hundreds of bats. We found four different bat species roosting in the cave and determined that the most numerous/dominant species was the Eastern bent-wing bat (*Miniopterus fuliginosus*). The other species were the Chinese pipistrelle (*Hypsugo pulveratus*), the greater horseshoe bat (*Rhinolophus ferrumequinum*), and the Chinese rufous horseshoe bat (*Rhinolophus sinicus*). These species identifications were confirmed by Dr. Tinglei Jiang (Northeastern Normal University, Changchun, China) who has surveyed to the cave in 2009. Some rare pulses that could match the great evening bat (*Ia io*, [101]) were also found in the recordings. The Institutional Animal Care and Use Committee (IACUC) of Virginia Tech approved this work (permit number #14-123) and the animal protection laws of the People's Republic of China were followed during the field work.

3.3.2 Field experiment setup

A camera (Gopro Hero 3+ Black with an IR-Pro IRP202 Hybrid lens) was set up approximately 2.5 m inside the cave from the entrance and oriented facing away from the entrance to monitor the flight activity in the cave entrance leading to the entrance (Fig. 3.1). The camera's field of view was lit by 12 infrared lights (SL-100IR 950 nm LED array illuminators). Six of the infrared lights were placed on the cave floor facing up and the other six were mounted on tripods at a height of approximately 1 m and oriented horizontally. The

volume over which bats could be detected in the camera images was limited by the infrared illumination and covered approximately 35 m^3. An ultrasonic recorder with an omnidirectional microphone (Wildlife Acoustics Song Meter SM2BAT+ ultrasonic recorder with SMX-UT microphone) was positioned on the ground about one third into the length of the camera's field of view and in the middle of its width (Fig. 3.1).

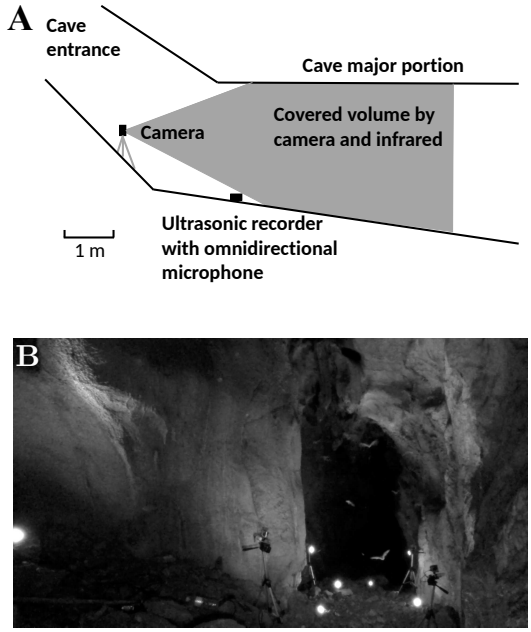

Figure 3.1: Field experiment setup in the cave. (a) Schematic layout of the setup (longitudinal section) (b) Example gray-scale frame from the video recording showing the setup. The bright spots are the infrared lights. Only the camera that produced this video frame was used for recording the data analyzed here – image data from the other cameras seen in the picture was not used for the present study.

3.3.3 Data set

All analyzed videos were recorded at a frame rate of 59.94 frames/second. Each video frame had a width of 1920 pixels and a height of 1080 pixels. The audio recording was acquired with a sampling rate of 384 000 samples/second and a resolution of 16 bit. The recorded audio waveforms were automatically normalized by the maximum absolute amplitude of the entire audio recording. Video and audio recordings commenced shortly after sunset (19:11pm) on 7/14/2014. Synchronization of video and audio was accomplished by producing audible impact sounds with two metal parts for ten times in the field of view of the camera. An recording period from 19:42-20:20pm for which video and audio were both available was selected for data processing. The analyzed data set hence contained $2306 \times 60 = 138\,360$ video frames spanning a period of 2308.30 seconds in total. Unless otherwise noted below, audio and video signals were processed in non-overlapping blocks of 60 video frames (1.001 seconds).

3.3.4 Video processing

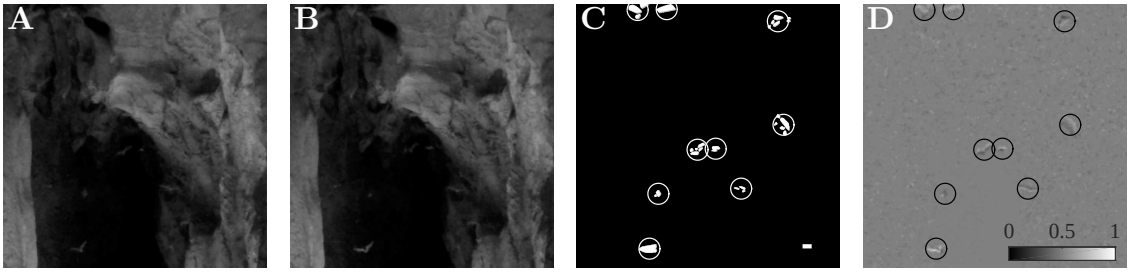

Figure 3.2: Bat identification. (a) and (b) Same part of two adjacent gray-scale frames which include all detected bats. (c) Automated bat identification. The black and white image was obtained by setting the brightness threshold on the absolute values of the frame difference between (a) and (b), and then eliminating the non-bat artifacts. Each white circle grouped the white regions whose nearest distances were less than the distance threshold (short white line at the bottom-right) and represented one bat. (d) Manual bat identification in the scaled frame difference. The black circles represented bats manually identified.

An automated method was developed to identify the bats in the video frames. In the first step, all the frames were converted from RGB color to 8-bit gray scale (Fig. 3.2(a), 3.2(b)). Next, the gray-scale pixel values of adjacent frames were subtracted to eliminate the static background. In this frame difference representation, a bat flying across the field of view

created adjacent regions with opposite signs of the change in gray scale. For example, if the bat was darker than its background, it would create a change from brighter to darker at its leading edge and a change in the opposite direction at its trailing edge. A fixed threshold (6% of the full gray scale) for the minimum absolute magnitude of these changes in brightness was set to select regions that could potentially contain bats. Candidate regions that were smaller than 35 pixels were eliminated as artifacts due to local change in brightness. If the nearest-neighbor distance between any of the remaining regions fell below a threshold of 15 pixels, they were grouped to represent a single bat (Fig. 3.2(c)). Finally, only those fused regions that contained positive as well as negative changes in brightness were interpreted to represent a bat to eliminate artifacts due to illumination changes on the scale of a bat.

The results of the automated method for bat detection were validated against manual counts that were conducted on frame-difference images that were scaled to maximize the contrast for the viewer (Fig. 3.2(d)). When conducting the manual counts, sequences of difference images were viewed to resolve ambiguous cases by considering motion trajectories.

The numbers of bats determined by the automated (N_b^a) and manual methods (N_b^m) for the same video images were compared for the third frame in every 60-frame block analyzed resulting in 2306 pairs of N_b^a and N_b^m estimates (Fig. 3.3). In general, the automated counts were close to the manual counts. However, the automated counts were slightly lower than the manual for large numbers of bats. This may be due to the fusion step of automated method that could result in regions belonging to different individuals passing each other being lumped together. For observer, the manual count was in a position to resolve such situations by scrolling back and forth in the sequence to identify multiple bats in a cluster from their flight trajectories.

The automated counting method was applied to 10 frames that were evenly spaced over each 60-frame block. From these 10 automated estimates, an average number of bats $\bar{N}_b^a$ for every 60-frame block was computed to obtain a more stable estimate. In addition, the spatial distribution of the bats over the cave cross-section was characterized by the mean and standard deviation of the vertical as well as horizontal locations of the identified bats in a chosen frame. The location of a bat was defined as the average pixel location of the grouped regions that represented the bat.

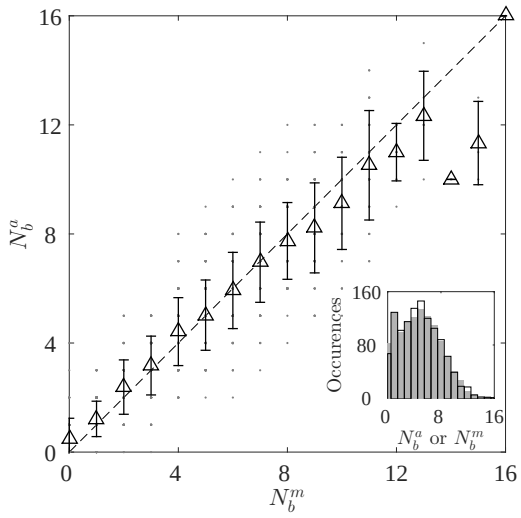

Figure 3.3: Comparison between automated ($\boldsymbol{N_b^a}$) and manual ($\boldsymbol{N_b^m}$) counts of the number of bats based on 2306 pairs of $\boldsymbol{N_b^a}$ and $\boldsymbol{N_b^m}$ estimates obtained from the same frame. Each triangular marker shows the mean of all N_b^a values for the same value of N_b^m. The error bars denote one standard deviation above and below the mean. The dashed line represents equality between N_b^a and N_b^m. The inset histograms shows the number of occurrences for the values of N_b^a (empty bars) and N_b^m (filled bars).

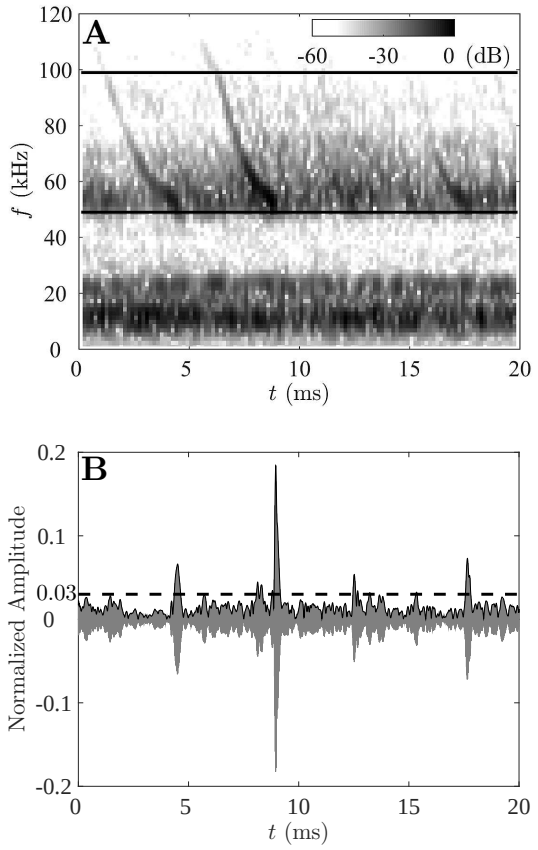

Figure 3.4: Audio processing. (a) Spectrogram representation of a sample audio recording. The horizontal line pair denotes the frequency band 49-99kHz for the Eastern bent-wing bats. (b) Normalized filtered signal of the sample recording after matched filtering using the artificial pulse template in Fig. 3.5. The wavy curve on top of the signal is the envelop. The dashed horizontal line denotes the threshold for pulse selection.

3.3.5 Audio processing

The audio data was surveyed using a spectrogram representation (Hamming window of length 256, 50% overlap, normalized to the amplitude maximum of the presented sequence, Fig. 3.4(a)). We defined the frequency band, 49-99 kHz, in the spectrogram for detecting pulses from the Eastern bent-wing bats.

A matched-filter was used to automatically detect pulses ascribed to the Eastern bent-wing bats. A time-reversed synthetic pulse that mimicked the instantaneous frequency and envelope amplitude functions of the bat pulses was used as the impulse response of the matched filter (Fig. 3.5). The output of the matched filter was normalized and envelop-detected (magnitude of the Hilbert transform). A constant amplitude threshold was used to detect signals (pulses or echoes) that matched the template (Fig. 3.4(b)).

The total in-band ultrasonic power p was calculated by summing over the power spectral density (linear scale) in 49-99 kHz for every 60-frame period (1.001 seconds) and then normalized. Power values lower than a background-noise threshold (10^{-10}) were excluded from the sum. The swarm pulse rate (number of pulses) N_p was defined as the number of identified pulses per every 60-frame period. The individual pulse rate n_p was defined as the swarm pulse rate N_p divided by the average number of bats $\bar{N}_b^a$ for the same 60-frame period, i.e., $n_p = \frac{N_p}{\bar{N}_b^a}$.

A Monte-Carlo simulation was used to investigate the relationship between the total in-band ultrasound power and the swarm pulse rate. A number of N_p^M synthetic bat pulses (Fig. 3.5) were distributed in a 60-frame period and added together to create a synthetic recording. For the synthetic recording, an ultrasonic power p^M was computed for the 49-99kHz band. For a fixed number of pulses N_p^M, we obtained 1000 p^M values by creating 1000 synthetic recordings. We varied N_p^M from 10 to 1600. The ultrasonic power p^M values were normalized using the overall maximum from the Monte-Carlo simulation. The software for the Monte-Carlo simulations and all data analysis steps was custom written using the MATLAB (The MathWorks, Inc., Natick, MA) numerical computing environment. The codes are available from the authors upon request.

3.4 Results

The average number of bats $\bar{N}_b^a$ rose to a maximum of about 14 and then declined to almost zero within the analyzed time period (Fig. 3.6). The maximum of 14 bats in the field of view of the camera corresponded to an average bat density of 0.4 $^{\text{bats}}/_{\text{m}^3}$.

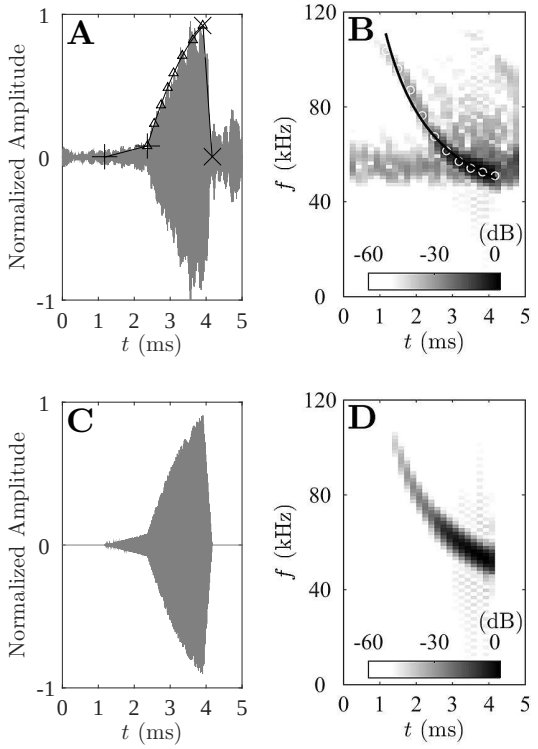

Figure 3.5: Synthetic bat pulse design for the Eastern bent-wing bat pulses. (a) Time-domain normalized signal of a recorded bat pulse. The pulse was pre-filtered using a Butterworth high-pass filter with the cutoff frequency at 47 kHz. The plus markers were connected by a straight line, so were the cross markers. The triangular markers were fitted using a quadratic function ($r^2 > 0.99$). (b) Spectrogram representation of the real bat pulse. The white circles were fitted using the inverse of a quadratic function (black curve, $r^2 = 0.98$). (c) Time-domain signal of the designed artificial bat pulse. (d) Spectrogram representation of the designed artificial bat pulse.

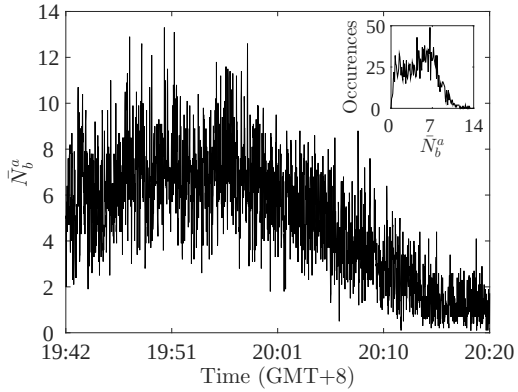

Figure 3.6: Average number of bats $\bar{N}_b^a$ over the time period used in the analysis. There are 2306 data points in the plot for the selected recording period of 2306×60 frames. Inset: number of data points for each $\bar{N}_b^a$.

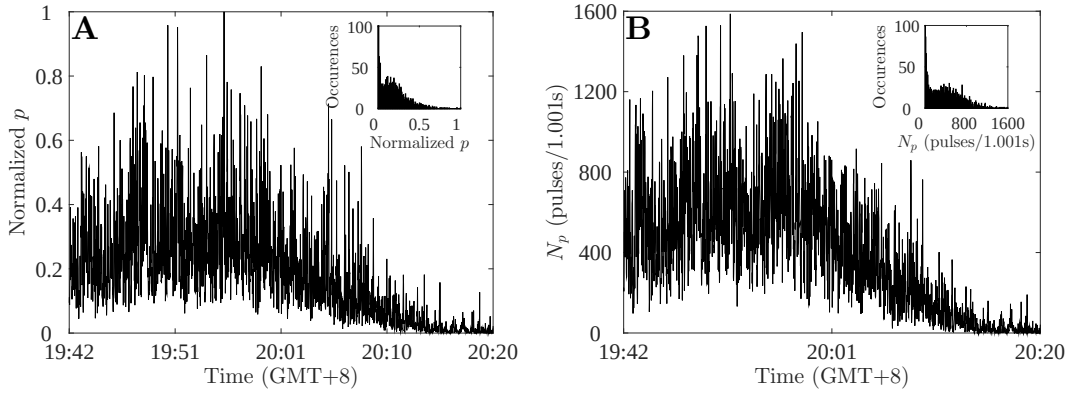

Figure 3.7: Time history of normalized ultrasonic power and swarm pulse rate for the analyzed audio recording. (a) The normalized ultrasonic power p. Inset: histogram of normalized p. (b) The swarm pulse rate N_p. Inset: histogram of N_p.

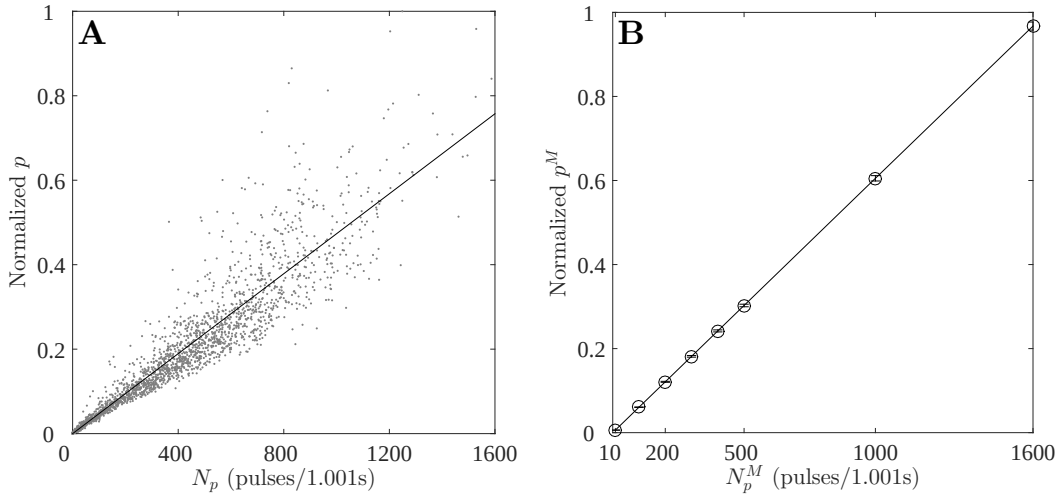

Figure 3.8: The relationship between ultrasound power and swarm pulse rate (number of pulses). (a) the normalized ultrasound power p as a function of swarm pulse rate N_p for the selected recording. There are 2306 data points with each representing a pair of normalized p and N_p values obtained for the same 60-frame period. Straight line: linear fit ($r^2 = 0.85$). (b) the normalized ultrasound power p^M as a function of the number of pulses N_p^M for the Monte-Carlo simulation. A circle denotes the mean of 1000 simulation values of normalized p^M for the same N_p^M. The error bar denotes one standard deviation above and below the mean.

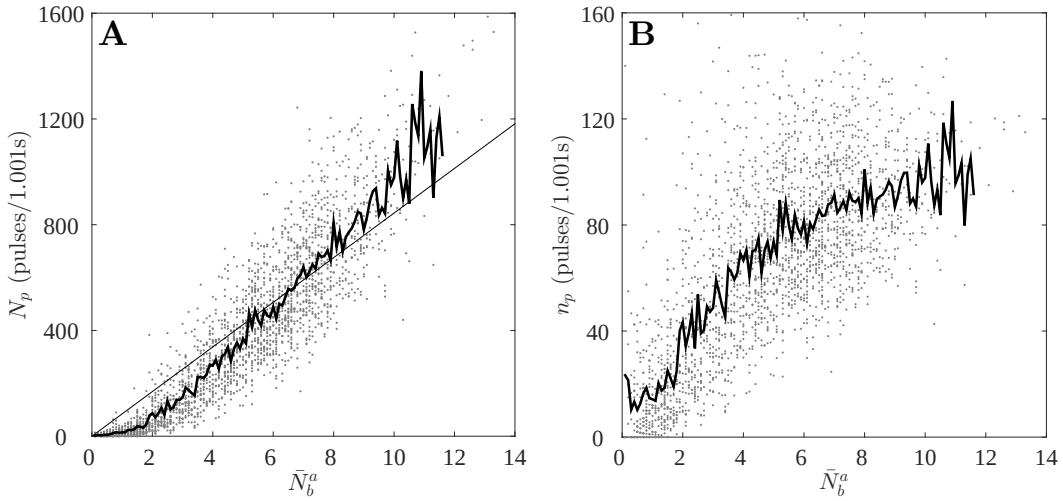

Figure 3.9: Bat pulse emission behavior for the Eastern bent-wing bat. (a) The swarm pulse rate N_p as a function of the average number of bats $\bar{N}_b^a$. Each data point represents a pair of N_p and $\bar{N}_b^a$ values for the same 60-frame period. Solid curve: mean of all N_p values for the same $\bar{N}_b^a$. Straight line: linear fit ($r^2 = 0.8$). (b) The individual pulse rate n_p as a function of the average number of bats $\bar{N}_b^a$. Each data point represents a pair of n_p and $\bar{N}_b^a$ values for the same 60-frame period. Solid curve: mean of all n_p values for the same $\bar{N}_b^a$.

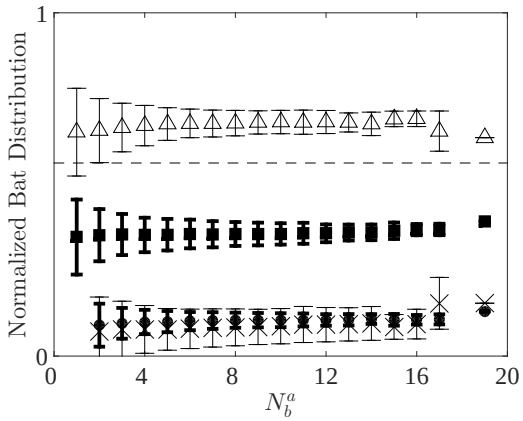

Figure 3.10: Bat distribution (normalized by the image width) as a function of the automated count of the number of bats $\boldsymbol{N_b^a}$. The filled square and circular markers show the averages of the means and standard deviations, respectively, of bat vertical locations for the same N_b^a. The triangular and cross markers show the averages of the means and standard deviations, respectively, of bat horizontal locations for the same N_b^a. The error bars denote one standard deviation above and below the averages. The thicker and thinner error bars are for bat vertical and horizontal locations, respectively. The dashed line denotes the image height.

A visual survey of the ultrasound recordings based on spectrogram representations did not yield any indications of qualitative changes in the pulses emitted by the bats over time. The pulses visible in the recordings followed a common pattern in terms of the occupied frequency band and time-frequency contours of the signals (Figs. 3.4(a) and 3.5(b)). All discernible Miniopterus pulses seemed to conform with biosonar pulses rather than social calls recorded from another Miniopterus species [102]. Hence, the result of the qualitative evaluation indicates that social calls were very rare compared to sonar pulses in this situation.

In a manner similar to the average number of bats, the total in-band normalized ultrasonic power p (Fig. 3.7(a)) and swarm pulse rate N_p (Fig. 3.7(b)) increased to a maximum and then declined to almost zero during the selected recording period. The total in-band ultrasonic power and the swarm pulse rate were found to be linearly correlated (Fig. 3.8(a)). This linear relationship between total pulse number and total ultrasonic power was reproduced by the Monte-Carlo simulation (Fig. 3.8(b)).

The swarm pulse rate N_p showed a monotonic increase with the average number of bats $\bar{N}_b^a$ that took an approximately sigmoidal form (Fig. 3.9(a)) with an initial region of slow growth (for $\bar{N}_b^a \leq 2$), a steep rise until an inflexion point (at $\bar{N}_b^a \approx 7$), and finally a region with declining slope beyond the inflexion point. The individual pulse rate n_p increased with average number of bats $\bar{N}_b^a$ but saturated for the larger values of $\bar{N}_b^a$ to a value of about 100 pulses per second (Fig. 3.9(b)). For the largest values of $\bar{N}_b^a$ in the data set, the curves of the mean values for N_p and n_p in Fig. 3.9(a) and 3.9(b) showed large variability due to the smaller number of data points for these extreme values (see the inset of Fig. 3.6).

The bat distribution – location (mean) as well the spread (standard deviation) – of bat pixel positions in the video images was found to be practically constant and did not change with the automated count of the number of bats N_b^a (Fig. 3.10). Hence, the data did not provide any evidence that the spatial distribution of the bats across the cave cross-section changed with an increase in the number of bats being present.

3.5 Discussion

The results reported here have demonstrated that Eastern bent-wing bats increase their biosonar output as their densities in a group increases. This was measured here as an increase in the individual pulse rate with increasing numbers of bats being present. Although well below the maximum pulse rates that have been reported for the buzz phase of echolocation sequences (up to 220 Hz, [103]), the individual pulse rates estimated from

the counts that were done here ($\sim$100 Hz) are unlikely to represent the actual output of the individual bats. Instead, they are likely to include strong echoes from the reverberant environment of the cave. However, these additional echoes should only effect the magnitude of the pulse count, but not the direction of the change that was observed with the number of bats.

The increased individual pulse rate that was counted with the approach used by the current study could have three different explanations: (i) it could correspond to an actual increase in the number of pulses, (ii) it could be that the bats increased their emission levels and that the resulting high-amplitude pulses were more likely to exceed the threshold that was set for counting the pulses, or (iii) it could be that for the larger numbers of bats, they flew closer to the microphone hence producing higher amplitudes and more signals that exceeded the threshold. The last hypothesis is contradicted by the results on the distribution of the bats within the camera's field of view. These results show that the bats usually stayed within a narrow flight corridor that did not change in location or width (standard deviation) as the number of bats increased. The remaining hypotheses (more pulses or pulses with higher amplitudes) are not mutually exclusive and could hence both be contributing factors to the observed effect.

The present findings differ from previous works that have shown a decrease of individual biosonar output of bats in groups. Groups of Mexican free-tailed bats (*Tadarida brasiliensis*) held in a small cage, for example, reduced their emission rates with increasing number of bats present [97]. Similarly, big brown bats (*Eptesicus fuscus*) flying in pairs in a flight room reduced their pulse emissions as the distances between the two bats decreased [24]. Besides the differences in the involved species, the situations under which these observations were made (e.g., field versus laboratory) were also very different and may be responsible for the different outcomes. It is not clear what the sensory needs of the animals in either of these situations might have been. There is ample evidence that bats increase their pulse rate in response to greater needs for sensory information [56, 104]. Having to fly in a group with an increasing number of individuals could create a need for a higher rate of sensory information that could be met through an increase in the pulse rate.

An increased pulse rate could also result in a greater probability of the bats in the group jamming each other. The maximum density estimated here based on the number of bats and the viewed volume was $0.4\,^{\text{bats}}/_{\text{m}^3}$, i.e., one bat in about $2.5\,\text{m}^3$. Evaluation of a numerical model for the acoustics of bat swarms [105] has suggested that such a density may not necessarily lead to serious jamming problem. With a sufficiently low duty cycle (less than 30%) and a narrow beam (40°), it was possible to achieve jamming probabilities below 3% [105]. The duty cycle of the Eastern bent-wing bats reported previously (about 10%, [106, 107]) would fit very well within these parameter ranges, no information on

the emission or reception beamwidth of these bats were found in the literature. Hence, a hypothesis that the bats in the recording situation increased their pulse rate to avoid collisions with other swarm members was possible because the jamming probability remained in an acceptably low range.

The main limitation of the present study is that it is based on averages across the entire swarm, for example, bat density estimates are derived from the number of bats in the total field of view without considering how the bats are distributed in three dimensions within this volume. To understand the situation and the echolocation behavior of the individual bats behind these averages, it would be desirable to reconstruct the three-dimensional trajectories of all the bats in the swarm. To obtain such reconstructions for substantial observation periods would require automated tracking methods that can handle solving the correspondence problem of matching individual bats across video frames from multiple cameras. Furthermore, it would be desirable to assign the individual biosonar pulses to the bats that have emitted them. This could be an even harder problem than solving the corresponding problem for the images of the bats, since the reverberant acoustics of the cave is going to make tracing sounds to their source difficult. Nevertheless, overcoming these difficulties may be worthwhile, because accurate information on the flight and acoustic situations of individual bats in swarms could open an avenue to understanding the strategies that the animals employ to deal with them.

Chapter 4

Bat pulse emission and swarm size - simulation

This chapter has been published in the Journal of Theoretical Biology with the title “Modeling perspectives on echolocation strategies inspired by bats flying in groups” [32].

4.1 Abstract

Bats navigating with echolocation- which is a type of active sensing achieved by interpreting echoes resulting from self-generated ultrasonic pulses- exhibit unique behaviors during group flight. While bats may benefit from eavesdropping on their peers’ echolocation, they also potentially suffer from confusion between their own and peers’ pulses, caused by an effect called frequency jamming. This hardship of group flight is supported by experimental observations of bats simplifying their sound-scape by shifting their pulse frequencies or suppressing echolocation altogether. Here, we investigate eavesdropping and varying pulse emission rate from a modeling perspective to understand these behaviors’ potential benefits and detriments. We define an agent-based model of echolocating bats avoiding collisions in a three-dimensional tunnel. Through simulation, we show that bats with reasonably accurate eavesdropping can reduce collisions compared to those neglecting information from peers. In large populations, bats minimize frequency jamming by decreasing pulse emission rate, while collision risk increases; conversely, increasing pulse emission rate minimizes collisions by allowing more sensing information generated per bat. These strategies offer benefits for both biological and engineered systems, since

frequency jamming is a concern in systems using active sensing.

4.2 Introduction

Species of bats in the suborder *Microchiroptera* are unique mammals that primarily navigate in their environment using echolocation [69]. They emit directional ultrasounds in pulses [55], receive reflected echoes to their auditory system through their deformable pinnae [108], and constantly interpret the echoes using a powerful neurological signal processing system [19, 109]. By analyzing echo harmonic structures, bats are able to differentiate targets from multiple sound reflections [110]. From a behaviorial perspective, many species of bats are highly social. They live in colonies that range from tens to millions of individuals [89, 87]. They may exhibit collective behavior [44] on fast time scales, such as their motion in group flight in the wild [87], and slower time scales, such as their roost selection dynamics [111]. Within their colonies, bats are able to fly in high densities [99, 90] at fast speeds [10], while avoiding collisions with peers and obstacles in the environment.

Bat group flight is a unique phenomenon that involves both complex sensing and behaviorial strategies. A major source of the complexity is bat's use of echolocation as an active sensing mechanism [20, 21] which allows interference from peers' sounds. The interference from active sensing can be both constructive and destructive, which is evidenced by bats' so-called eavesdropping and frequency jamming avoidance behaviors, respectively. Eavesdropping behavior is defined as bats listening and reacting to peers' pulses and echoes [23, 24] in situations wherein they do or do not emit pulses. Frequency jamming happens when bats emit pulses of frequencies that overlap the frequency bandwidth of peers' pulses, which may be inevitable for bats flying in large groups in natural settings [99, 90, 10]. It has been demonstrated that bats are able to shift the frequencies of their ultrasounds in situations tailored to produce jamming [26, 27, 28], thus avoiding potentially destructive interference, and recent work has shown incidences of offensive jamming between wild bats during hunting which may necessitate such accommodations [112]. Bats are also observed to cease vocalization in the presence of peers in laboratory settings [24, 97], which may allow them to simultaneously eavesdrop on peers' information and avoid jamming. There are currently few studies, however, documenting bats' behavior during flight in the wild and in dense groups.

Mathematically, animal behavior can be modeled as a multi-agent system, where each agent in the group is subject to behavioral rules [57]. Collective behavior at the group

level, such as fish schooling [7, 113], bird flocking [8] and ant lane formation [9], may be simulated using these so-called agent-based models when agents are equipped with specific sensing and response schemes [11]. Rules prescribed to individuals for collective behavior may include repulsion from peers, alignment of velocity directions, and attraction to peers' positions [12, 13]. These rules are realized in models by building either discrete decision-making [57, 12, 13] or potential functions [48]. Agent-based modeling is also applied to study multi-agent systems in other disciplines, such as population dynamics [50, 51], predation-prey interactions [114, 115, 29], cell chain migration [116], and disease or parasite transmission [117, 118].

In this work, we establish an agent-based model to study echolocation strategies which include eavesdropping and changing pulse emission rate inspired by bats emerging from a cave. In the model, bats are designed to fly through a three-dimensional tunnel of rectangular cross-section while avoiding collisions with peers and boundaries, referred to as obstacles. They emit pulses of unique frequencies, and use echoes generated by their own pulses and eavesdropped echoes and pulses from peers to locate obstacles. We note that, although bats echolocate in nature using diverse calls that may be constant frequency or frequency modulated, the acoustic signature of calls are not considered in this model since time is discretized into steps which each can contain a single call. Bats in the model obtain exact obstacle locations with their own pulses, while they estimate obstacle locations using echoes and pulses from their peers perturbed by random noise with a fixed probability distribution; we call this penalty on eavesdropping "measurement noise". In a simulation study, we find that eavesdropping is beneficial in collision avoidance when measurement noise is low. In this case, bat pulse emission rate is balanced between emitting pulses to reliably avoid collisions and varying pulse emission rate to avoid frequency jamming and conserve energy for echolocation, which is quantified using defined cost functions relevant to both biological and engineered systems. This model may help better understand bats' group behavior and inspire control algorithms for robotic teams that use active sensing [2, 3].

4.3 Modeling

4.3.1 Model description

In the following, we describe the model for the acoustic field generation and for bat behavior.

Sensing setup

We consider an agent-based model with the agents, "bats", flying through a three-dimensional tunnel using echolocation and tasked with collision avoidance. The N bats are modeled as self-propelled particles moving with a constant velocity magnitude s in discrete time. The three-dimensional tunnel is a cuboid with side lengths L_x, L_y and L_z, which are the width, length and height of the tunnel, respectively. To model echolocation, we consider that each bat emits a pulse of a unique frequency according to an independent, identically distributed Bernoulli random variable with a constant pulse emission probability p at each time step. The pulse is considered to cover a three-dimensional sensing space, a spherical cone, inspired by a simplified bat sonar beam pattern [55, 110, 56]. The apex of the spherical cone is the bat's position; its side length equals the bat's sensing range r_s; and its opening angle is the bat's angular range of sensing ϕ. The bat's velocity vector originates at the spherical cone's apex and aligns with its central axis. We define a repulsion zone as a sphere of radius r_r centered at the bat's position. Peers and boundaries with positions in this zone are considered to be obstacles and are perceived by the bat as too close, so the bat performs a collision avoidance maneuver. A schematic of the sensing space and the repulsion zone for bat i, $i = 1, 2, \ldots, N$, is shown in Figure 4.1.

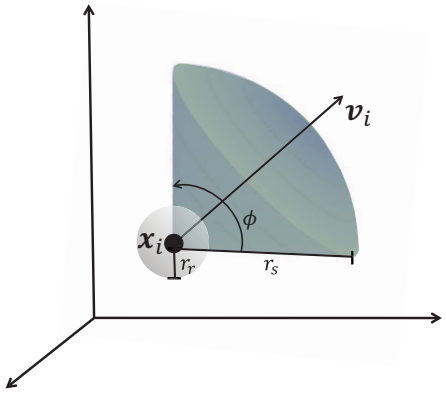

Figure 4.1: Schematic of three-dimensional sensing space and repulsion zone for bat i. The bat has position $\boldsymbol{x}_i$ and velocity $\boldsymbol{v}_i$. The spherical cone shows the bat's sensing space with sensing range r_s and angular range of sensing ϕ. The gray sphere shows the bat's repulsion zone with radius r_r.

Echo generation

When a bat emits a pulse at a given time step, echoes are reflected from peers and boundaries that occupy the bat's sensing space simultaneously. These echoes are considered as the bat's "self echoes" as they result from the bat's pulse. Echoes generated by pulses from peers in the group are called "peers' echoes". Echoes exist for a single time step and they occupy spherical cones of a constant radius r_e, with boundaries producing hemispherical echoes with opening angles of π radians and peers producing conical echoes with opening angles of $\pi/2$ radians. The emitted pulses and reflected echoes are both considered to be incident at the same time step, since we select a discrete time step large enough for sound to propagate through the full echo hemisphere.

We define cases for echoes reflected from peers and boundaries separately. In the first case, a bat's sensing space is considered to be occupied by a peer if the distance between the bat and the peer is less than r_s and the angle between the vector from the bat to the peer and the bat's velocity is less than $\phi/2$. In this case, if the bat emits a pulse, a conical echo is simultaneously reflected from the peer with its base centering at the peer's position and its central axis connecting the bat and the peer; the dome of the echo is directed toward the bat emitting the pulse. In the second case, a bat's sensing space is occupied by a boundary, so we can find the cross-section of the sensing cone that passes through the cone's central axis and is orthogonal to the two-dimensional boundary. The intersection of this cross-section with the boundary is a line segment. We consider that a hemispherical echo originates from the point on the line segment which is nearest to the bat's position. The base of the hemispherical echo is on the boundary and the dome is inside the tunnel. If the bat's sensing space is occupied by multiple boundaries, echoes are reflected from each intersecting boundary independently.

Echo interpretation

While a bat's sonar emission is directional according to the geometry of the conical sensing space described above, its sonar reception is omnidirectional, that is, bats can receive sounds from any angular position. A bat is designed to use all sound information (echoes and pulses) it "hears" to locate obstacles, where hearing is defined in the following. A bat is considered to hear an echo if the bat occupies the conical echo volume, which means the distance between the echo base center and the bat's position is less than r_e and the angle between the vector from the echo center to the bat and the echo's central axis is less than $\pi/4$ radians for echoes from peers and $\pi/2$ radians for echoes from boundaries. A bat is considered to hear a pulse from a peer if the bat occupies the peer's sensing space. The

obstacle locations in the model are taken as the apexes of the echoes when the bat hears echoes or the positions of peers whose sensing space is occupied by the bat when the bat hears peers' pulses.

We enable bats to distinguish between self information, which are self echoes, and peers' information, which are peers' echoes and pulses, since bats are considered to emit pulses of unique frequencies. Bats are able to obtain exact obstacle locations by hearing self echoes reflecting from them, while they obtain perturbed obstacle locations by hearing peers' echoes or pulses. This perturbation is designed as penalty motivated by the fact that bats lack timing information for peers' information in nature. The perturbed location is on the line segment of length r_e that connects the bat and the obstacle's exact location. The distance between the bat and the perturbed location is a random number that has a Gaussian distribution with the exact distance from the bat to the obstacle as the mean and a perturbation parameter η_d as the standard deviation. Since the distance between the bat and the perturbed location is restricted in the interval $[0, r_e]$, we only use realizations of the Gaussian distribution which give random values that belong to the stated interval; otherwise, the random variable value is regenerated.

This model of echo generation and interpretation simplifies the acoustic interactions that occur between bats and their environment. For example, we do not consider echo scattering as a result of an obstacle's surface roughness, which may confound locating the echo source. These simplifications can be eliminated by increasing detail of the model environment and the resulting acoustic field, which would greatly increase the model's computational complexity. Since we seek to identify macroscopic group behaviors, we neglect these details and instead add a random noise to the bat behavior model detailed in the following.

4.3.2 Position and velocity updates

The update for the position of bat i, x_i, is defined at time $t + \Delta t$ as

$$\boldsymbol{x}_i(t + \Delta t) = \boldsymbol{x}_i(t) + \boldsymbol{v}_i(t + \Delta t)\, \Delta t, \tag{4.1}$$

where $t \in \mathbb{R}^+$, $\Delta t \in \mathbb{R}^+$ is the constant time step, and $\boldsymbol{x}_i,\ \boldsymbol{v}_i \in \mathbb{R}^3$ are the bat's position and velocity vectors, respectively. The velocity in this equation is updated with the goal of the bats avoiding collisions with peers or the domain boundaries.

Specifically, we update bat i's velocity based on the bat's previous velocity direction, the preferred tunnel direction and a repulsion force from obstacles. The previous velocity

direction is the base direction from which the bat turns and ensures the smoothness of the bat's flight trajectory; the preferred tunnel direction describes an external motivation for the bat's flight; and the repulsion force enables the bat to reduce collision risk with peers or boundaries. In particular, the velocity update for bat i at time $t + \Delta t$ is

$$\boldsymbol{v}_i(t + \Delta t) = s\frac{\boldsymbol{\mathcal{R}}^{\eta}[\alpha\, \boldsymbol{v}_i(t)/s + \beta\, \boldsymbol{y} + \gamma\, \boldsymbol{r}_i(t)/\|\boldsymbol{r}_i(t)\|]}{\|\boldsymbol{\mathcal{R}}^{\eta}[\alpha\, \boldsymbol{v}_i(t)/s + \beta\, \boldsymbol{y} + \gamma\, \boldsymbol{r}_i(t)/\|\boldsymbol{r}_i(t)\|]\|} \tag{4.2}$$

where $\boldsymbol{y} = [0, 1, 0]$ is the constant unit vector representing the preferred tunnel direction, α, β and γ are weighting coefficients describing the velocity update's dependence on the three summands, and $\boldsymbol{\mathcal{R}}^{\eta}[\bullet]$ denotes an operator which perturbs a three-dimensional vector in a random direction uniformly distributed in the plane normal to it with a Gaussian-distributed random angle. The Gaussian distribution of this perturbation has mean zero and standard deviation $\eta\pi$ with its value restricted in the interval $[0, \eta\pi]$. Here, η is a parameter that describes how well a bat adheres to the model's desired direction $\alpha\, \boldsymbol{v}_i(t)/s + \beta\, \boldsymbol{y} + \gamma\, \boldsymbol{r}_i(t)/\|\boldsymbol{r}_i(t)\|$ in the next time step, and can be interpreted as a noise on both the bat's sensing and decision making. The values of η range from 0 to 1, where 0 means that bat i updates velocity in the desired direction and 1 indicates that bat i's velocity update can be in any direction in the unit sphere.

The repulsion force $\boldsymbol{r}_i(t)$ is given by

$$\boldsymbol{r}_i(t) = \boldsymbol{x}_i(t) - \frac{1}{|\mathcal{N}_i(t)|}\sum_{j=1}^{|\mathcal{N}_i(t)|} \boldsymbol{y}_j(t) \tag{4.3}$$

where $\mathcal{N}_i(t)$ is the set of indices of obstacle locations in bat i's repulsion zone at time step t, denoted as $\boldsymbol{y}_j(t) \in \mathbb{R}^3$, and $|\bullet|$ is set cardinality. Obstacles locations are accurate if obtained by bat i using self echoes or perturbed if estimated by bat i using peers' echoes and pulses. Thus, the repulsion force direction is determined by the average relative position of obstacle locations in $\mathcal{N}_i(t)$. Note that a bat may use both exact and perturbed locations of the same obstacle for velocity update, which occurs when the bat obtains both self and peers' information about an obstacle. When $\mathcal{N}_i(t) = \emptyset$, the term $\boldsymbol{r}_i(t)/\|\boldsymbol{r}_i(t)\| = [0, 0, 0]$; this means that the repulsion force is zero when there are no exact or perturbed obstacle locations in bat i's repulsion zone. A flow chart that illustrates eavesdropping bats' behavior is shown in Figure 4.2. We comment that, in order to evaluate the benefit of eavesdropping behavior, we define the case of no eavesdropping when bats do not use peers' echoes or pulses and fly independently. In this case, $\mathcal{N}_i(t)$ is the set of indices of exact obstacle locations obtained by bat i using self pulses.

Bats' initial positions and velocity directions are generated with uniform probability in the tunnel and in $\mathbb{R}^3$, respectively. We consider periodic boundary conditions for the tunnel

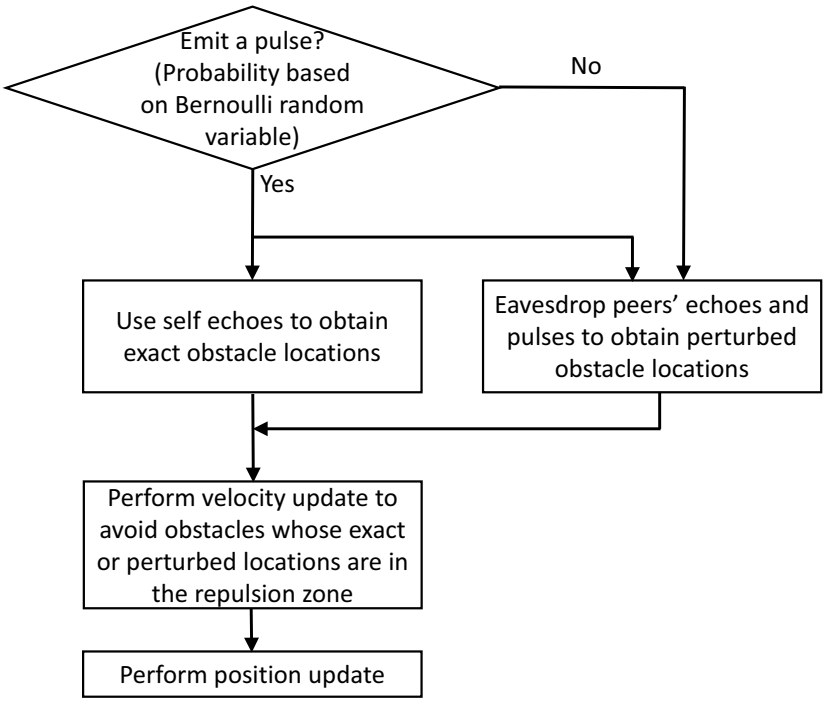

Figure 4.2: Flow chart that summarizes the decision making and behavior of a bat at each time step.

faces which are orthogonal to the L_y direction. The boundary conditions orthogonal to the L_x and L_z directions are considered as reflective which means, if the position update defines a position outside a face orthogonal to L_x or L_z direction, this position is replaced by another one symmetric about the face at the same time step. In this manner, the bats' positions are ensured to be inside the finite domain.

4.4 Observables

We define three observables to measure the behavior of the bat group: the average collision rate c, the collision/jamming cost s_1, and the collision/energy cost s_2. The average collision rate measures the collision avoidance failure of the bat group. The two cost functions are defined to consider natural and engineering settings, respectively. The collision/jamming cost combines average collision rate and potential for frequency jamming, as the frequency band-widths of bats' pulses overlap in natural bat swarm. The collision/energy cost combines average collision rate and energy use per bat, as engineered agents are able to use unique frequencies in their signals but have limited power sources for sensing. Energy is only considered to be used for sensing in this model.

The average collision rate is calculated as the sum of number of bats colliding with peers or boundaries over time divided by the number of bats N and by the total number of time steps T. A bat is defined to collide with a peer if the distance between them is less than the peer collision range r_c and with boundaries when the reflective boundary conditions for the L_x and L_z directions are used. Thus,

$$c = \frac{\sum_{t=1}^{T} n_c(t)}{NT}, \tag{4.4}$$

where $n_c(t)$ is the number of bats colliding with peers or boundaries at time t.

The collision/jamming cost s_1 is defined as the weighted sum of the average collision rate c and the average number of pulses over the group Np. The average number of pulses represents the extent of frequency jamming, because a more cluttered acoustic field makes it more difficult for a bat to emit a pulse of a unique frequency in nature. In particular,

$$s_1 = c + \zeta_1 Np, \tag{4.5}$$

where ζ_1 is the weighting coefficient for frequency jamming.

The collision/energy cost s_2 is computed as the weighted sum of the average collision rate c and the pulse emission rate p, as the pulse emission rate conveys the average energy use

Table 4.1: Parameter values used in the simulation study.

Parameter	Symbol	Value	Unit
Width of the tunnel	L_x	5	m
Length of the tunnel	L_y	15	m
Height of the tunnel	L_z	5	m
Time step	Δt	0.1	s
Number of bats	N	$2-100$	-
Bats' velocity magnitude	-	5	$\mathrm{m/s}$
	s	0.5	$\mathrm{m}/\Delta\mathrm{t}$
Bats' sensing range	r_s	5	m
Bats' angular range of sensing	ϕ	$2\pi/3$	rad
Echo radius	r_e	5	m
Perturbation parameter for estimating obstacle locations	η_d	$0-+\infty$	-
Perturbation parameter for bat swarming	η	0.1	-
Pulse emission probability	p	$0-1$	-
Weighting coefficient for previous velocity direction	α	1	-
Weighting coefficient for preferred tunnel direction	β	0.3	-
Weighting coefficient for repulsion force direction	γ	1	-
Bats' repulsion zone radius	r_r	0.6	m
Bats' collision range	r_c	0.3	m
Weighting coefficient for frequency jamming	ζ_1	2×10^{-4}	-
Weighting coefficient for energy use per bat	ζ_2	10^{-2}	-

per bat. In other words,

$$s_2 = c + \zeta_2 p, \tag{4.6}$$

where ζ_2 is the weighting coefficient for energy use per bat. Note that small and large values of s_1 or s_2 indicate relatively low and high costs, respectively. We comment that any energy bats use for echolocation may be negligible compared to the high energetic cost of flight [119, 120]. However, the energy used by active sensors in engineered systems is certainly non-trivial, which motivates this observable.

4.5 Simulation results

We determine the parameter values for the model by taking inspiration from bats emerging from caves in natural settings. We set the nominal width, length, and height of the

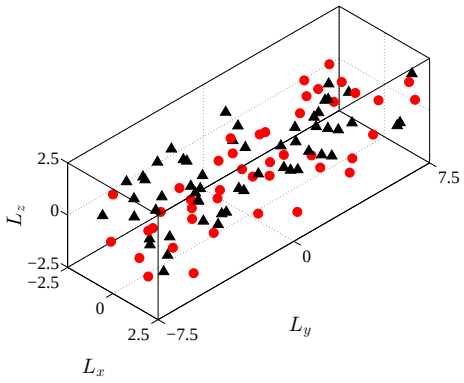

Figure 4.3: Example frame of $N = 100$ bats flying through the tunnel with $p = 0.5$ and $\eta_d = 0$. Red circles and black triangles show positions of bats emitting pulses and ceasing emission, respectively. The units for the axes are meters.

Table 4.2: Simulation replicate length.

N	Replicate length (time steps)
2	500 000
5	200 000
10	100 000
20	25 000
50	5 000
100	2 000

tunnel to be $L_x = 5\mathrm{m}$, $L_y = 15\mathrm{m}$ and $L_z = 5\mathrm{m}$, respectively. We consider the physical parameters of big brown bats, *Eptesicus fuscus*, in the model as they are common in North America and have been widely studied in the biological literature [121]. Big brown bats emit echolocation calls on the order of 10 times per second [69], which defines the time step $\Delta t = 0.1\mathrm{s}$. In the model, bats are considered to emit pulses and use all received information to perform navigational decisions at one time step. Big brown bats detect small targets that are within $5\mathrm{m}$ range [110, 68]; thus, we set both the sensing range r_s and echo radius r_e to be $5\mathrm{m}$. Bats' angular range of sensing is taken to be $2\pi/3$ radians according to the sonar beam pattern of big brown bats [55, 110]. Bats' velocity magnitude is set to be $5\mathrm{m/s}$, which is considered as the nominal flying speed of big brown bats [69]. The collision range among bats is chosen as the approximate average wingspan of big brown bats, which is $r_c = 0.3\mathrm{m}$ [122]. We set the repulsion zone radius to be twice the collision range as $r_r = 2r_c = 0.6\mathrm{m}$, which is considered to be a safe distance for bats to avoid collisions with both peers and boundaries.

The perturbation parameter for bat swarming is defined as $\eta = 0.1$, which adds a small error to a bat's desired swarming direction. The weighting coefficients in the velocity update for previous velocity direction, preferred tunnel direction and repulsion force direction are taken to be $\alpha = 1$, $\beta = 0.3$ and $\gamma = 1$, respectively, based on inspection of preliminary simulations. The selected dependence of velocity update on the previous velocity direction results in relatively smooth flight trajectories, which matches well with natural bat flight patterns [70, 71]; the relatively small weighting coefficient for the preferred tunnel direction reduces the straightness of bats' flights in the tunnel direction, while enforcing flight through the tunnel on average; and the selected dependance on the repulsion force direction results in good collision avoidance performance as bats avoid obstacles without blocking peers' flight paths.

In the simulation, bats move subject to the rules defined in the Modeling section with the numbers of bats N taken as 2, 10, 20, 50, and 100; the pulse emission probability p as 0, 0.1, 0.2, 0.3, 0.4, 0.5, 0.6, 0.7, 0.8, 0.9, and 1; and the perturbation parameter for estimating obstacle locations η_d as 0, 0.1, 1, 2, 10 and $+\infty$. We comment that, when $\eta_d = 0$, bats obtain the exact obstacle locations using peers' information; when $\eta_d = +\infty$, the estimated obstacle locations are uniformly distributed along the line segment of length r_e that connects the bat and the obstacle's exact location. Figure 4.3 shows an example frame of 100 bats swarming in the simulation with $p = 0.5$ and $\eta_d = 0$. In calculating the two flight costs, we set the weighting coefficient for frequency jamming as $\zeta_1 = 2 \times 10^{-4}$ and the weighting coefficient for energy use per bat as $\zeta_2 = 10^{-2}$, such that the two summands are approximately equal in magnitude within each cost function. Table 4.1 gives a summary of all the parameter values used in the simulation study.

For the numerical study, we determine the simulation length for each combination of N, p and η_d values by considering a constant initial transient phase of 1000 time steps and 10 simulation replicates whose length is determined by N. The initial transient phase is confirmed to be sufficiently long to exclude the influence of initial conditions by inspecting the time series of the average collision rate for all cases. For each case of N, p and η_d, we compute the average collision rate for each replicate and obtain the mean and standard deviation for the average collision rate over the 10 replicates. We ensure the stationarity of the results by checking that the standard deviation divided by the mean is less than 10%. Table 4.2 shows the length of one simulation replicate for each N. For larger N, the replicate length reduces because collisions occur with higher probability and the average collision rate approaches steady state faster.

As we vary the three free parameters in the model, we only present a subset of the results that enable understanding the behavior of bats flying in groups. Figure 4.4 shows the average collision rate c versus the number of bats N with varying η_d values for a fixed $p = 0.5$; simulations with different p values show similar trends and are thus not shown. In Figure 4.4, we see that the average collision rate increases as the number of bats increases for all η_d values. For $\eta_d = 0$ and $\eta_d = 0.1$, the average collision rates are practically equal and both smaller than that for no eavesdropping and, for $\eta_d \geq 1$, the average collision rates have larger values than that for no eavesdropping.

We investigate the benefit of eavesdropping through comparison with the situation when bats do not use peers' information and fly independently. We use the case of $\eta_d = 0$ to represent the cases with $\eta_d \leq 0.1$, wherein the average collision rates are smaller than that for no eavesdropping as shown in Figure 4.4. Figure 4.5(a) is a contour plot of the average collision rate for $\eta_d = 0$ with varying N and p. From this figure, we see that the average collision rate increases as p decreases and N increases. Figure 4.5(b) is a contour plot of the ratio between the average collision rate with $\eta_d = 0$ and that for no eavesdropping; it shows that this ratio is smaller for larger bat populations and higher p values.

The collision/jamming and collision/energy costs for $\eta_d = 0$ with varying N and p are shown in the contour plots in Figures 4.6(a) and 4.6(b), respectively. From Figure 4.6(a), for a bat population of fixed size, the collision/jamming cost shows a non-monotonic trend as p decreases. The "optimal" pulse emission rate associated with the minimum cost for each N is connected through a red curve on the contour plot, showing a decreasing trend as N increases in general. We also consider the scenario that bats may seek to keep the same cost as group size increases, so we find p values that correspond to a constant s_1. For example, such p values for a constant cost of $\log_{10}(s_1) = -2.8$ are connected through the red dotted curve for $N \leq 6$ in Figure 4.6(a) and show an increasing trend. For larger populations with $N > 6$, bats are not able to continue to achieve this constant cost. A

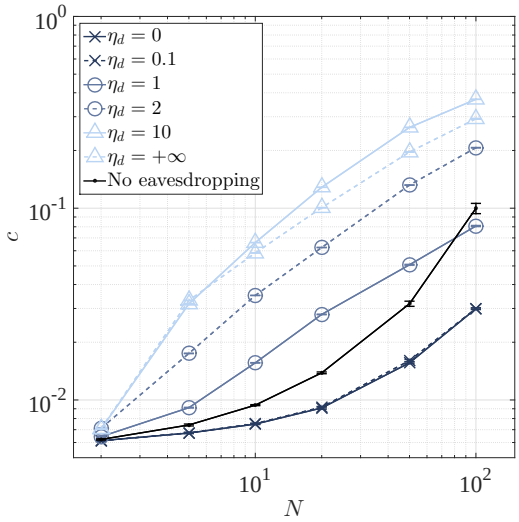

Figure 4.4: Average collision rate c versus the number of bats N with varying η_d values for $p = 0.5$ and with the case of no eavesdropping. Error bars showing one standard deviation over the ten replicates are plotted at every point, but are occluded by point markers due to their very small magnitude in almost all cases.

similar trend occurs for other different constant s_1 values. From Figure 4.6(b), we see that the collision/energy cost has an analogous nonmonotonic trend for fixed N and varying p. However, the optimal pulse emission rate increases with increasing N, as shown by the blue curve.

4.6 Discussion

Based on the simulation study, we obtain the following observations regarding bats swarming in groups: (i) if bats are able to estimate obstacle locations using peers' information with low measurement noise, eavesdropping is a better option than flying independently in terms of collision avoidance; (ii) bats are able to suppress pulse emission to accommodate frequency jamming although the collision risk increases; and (iii) bats may increase pulse emission rate to achieve better collision avoidance performance while using more energy individually.

The eavesdropping rule enables bats to use peers' echoes and pulses to obtain information about surrounding obstacles, which is beneficial when the measurement noise is low. In

the model, bats emit directional pulses with which they only sense their environment in the flying direction. With eavesdropping, bats are able to estimate locations of obstacles which are not covered by their sensing space. Moreover, if bats cease pulse emission which may occur when $p < 1$, they receive information about the surrounding environment without generating a signal. Successful collision avoidance may be helped or hindered by this extra information, depending on its accuracy, namely low or high measurement noise. For low noise up to $\eta_d = 0.1$, bats' collision avoidance performance is comparable to $\eta_d = 0$, that is, when bats obtain the exact locations of obstacles from peers. For higher noise with $\eta_d \geq 1$, the estimated obstacle locations are more likely to be perturbed along the limited sound propagation distance that connects the bat and obstacle, which may result in incorrect velocity update decisions that cause more collisions. This is expected to model the biological system since eavesdropping bats garner directional information, but lack time-of-flight, from peers' echoes and pulses. However, the literature is lacking quantitative studies of this potential effect. We comment that bats are known to exhibit aligned flight formations [90] which may enable them to eavesdrop with low measurement noise due to regular patterns of following flight [24]. The benefit of eavesdropping is evidenced in Figure 4.5(b), where we observe bats having fewer collisions when they eavesdrop with low noise than flying independently. This benefit increases with bat population as bats obtain more information about obstacles from the increasing number of surrounding peers. When the pulse emission rate p reduces, the benefit of eavesdropping vanishes as there are fewer echoes and pulses in the domain. We note that this feature relies on the model's simplification that bats are able to process many signals simultaneously; however, bats perception of numerous signals may be limited in real environments.

Suppressing pulse emission reduces the amount of information in acoustic field, which results in less frequency jamming and lower collision/jamming cost when bats eavesdrop with low measurement noise. With low measurement noise (i.e. situations where eavesdropping is beneficial), the average collision rate increases as p reduces because there is less sound information available for bats to avoid obstacles, see Figure 4.5(a). We note that this trend is reversed when bats use peers' information with high measurement noise, due to the destructive influence from high measurement noise causing more collisions for larger p values. Generally speaking, the chance of experiencing frequency jamming in a real system increases for larger N and p values, because the frequency of a bat's emitted pulse is more likely to overlap peers' pulse frequency since there are more pulses overall. The minimum collision/jamming cost occurs at an optimal value of $p < 1$, which captures the benefit of ceasing vocalization for frequency jamming avoidance documented by behavioral studies on big brown and Mexican free-tailed bats [24, 97]. This optimal pulse emission rate decreases with N because frequency jamming dominates the collision/jamming cost for larger bat populations. The benefit of ceasing vocalization is also

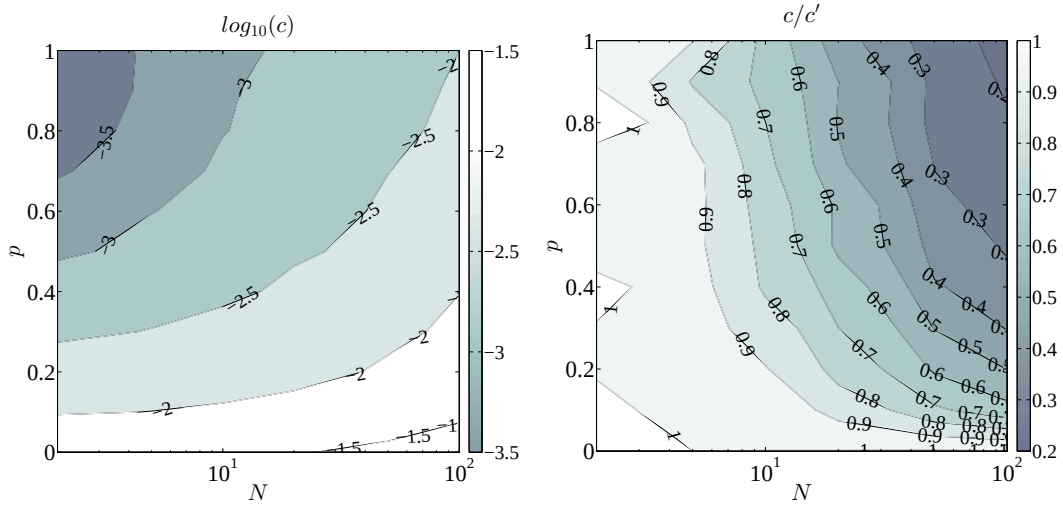

Figure 4.5: (a) The average collision rate c with varying N and p for $\eta_d = 0$; (b) the ratio between the average collision rate with $\eta_d = 0$ and the average collision rate with no eavesdropping. Here, c' denotes the average collision rate for simulations with no eavesdropping, which has similar trends as in (a) but with larger values.

observed in the case of no eavesdropping, where the optimal p is higher due to its larger average collision rate values as compared to the case with eavesdropping. We comment that the bat group uses less energy on average when individuals reduce their pulse emission rate, which may have benefits beyond frequency jamming avoidance. However, we do not include energy consumption per bat in determining bat group behavior in natural settings because it may be a less immediate danger than the risk of collision from frequency jamming; this priority is motivated by engineering applications of this work, since the balance between energy use and collision risk is a dynamic and multifaceted problem for animals and cannot be decisively categorized. We also note that bats may not experience any frequency jamming in very sparse groups in natural settings, which allows for increasing pulse emission rate while keeping a constant safety margin in small populations as shown by the red curve in Figure 4.6(a).

The optimal pulse emission rate for minimizing collision/energy cost increases with bat population, as bats obtain greater benefit in collision avoidance by eavesdropping peers' information with low measurement noise, see Figure 4.6(b). The very low average collision rate for larger bat groups with high pulse emission rate, shown in Figure 4.5(a), results in low collision/energy cost while the energy use per bat given by p increases. In general,

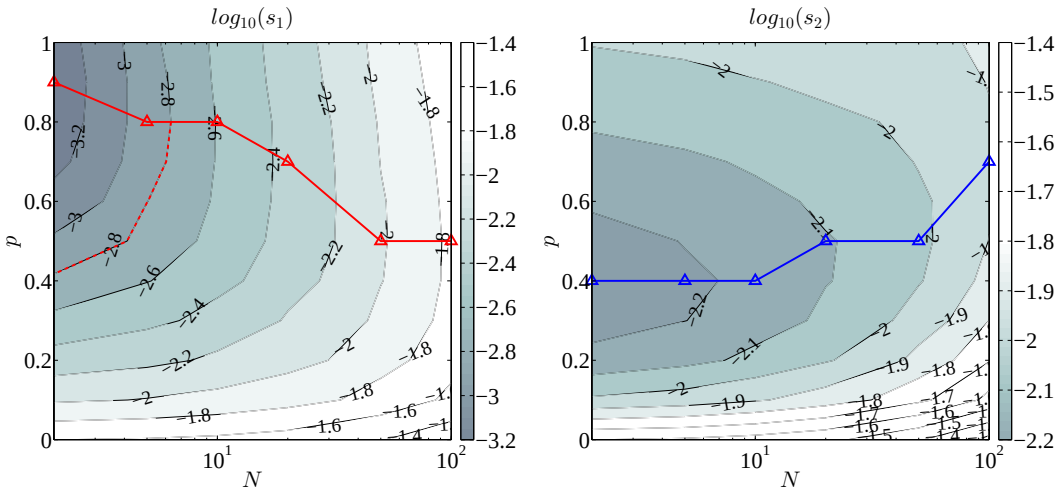

Figure 4.6: (a) The collision/jamming cost s_1 and (b) the collision/energy cost s_2 with varying N and p for $\eta_d = 0$. In (a), the red curve denotes the minimum collision/jamming cost for different N; the red dotted curve shows the pulse emission rates corresponding to a constant collision/jamming cost $\log_{10}(s_1) = -2.8$ for $N \leq 6$. In (b), the blue curve denotes the minimum collision/energy cost for different N.

the optimal pulse emission rate resulting from increased energy use per bat and decreased collision risk suggests that there is an attainable balance of avoiding collisions and saving energy in engineered systems with analogous acoustic capabilities. In such a system, this tradeoff may be tuned using the weighting coefficient in the collision/energy cost. We comment that, if we consider the total energy use of the bat group given by Np instead of the energy use per bat in calculating the collision/energy cost, we see a decreasing optimal pulse emission rate, which is the same as the collision/jamming cost.

In conclusion, information sharing among agents in groups and changing pulse emission rate are possible active sensing strategies in nature and in engineering. Using peers' information by eavesdropping may provide substantial benefits for groups in terms of collision avoidance, frequency jamming avoidance and energy saving. Reducing or increasing pulse emission rate, on the other hand, balances collision and jamming avoidance or collision and individual energy use, respectively. We comment that the actual behavior of bats flying in groups in nature may be different from the modeling results. For example, bats may increase pulse emission rate to find unique pulse frequencies as a response to frequency jamming in large groups. In addition, individuals may combine information from peer's pulses and their echoes to lessen timing uncertainty when performing passive sonar. Future work includes obtaining the relationship between the pulse emission rate and the bat population in field studies on wild bat swarms to elucidate behaviors dictating pulse emission strategies, as well as tying these behaviors to the physical acoustic accommodations that bats must make to use variable frequencies for echolocation. We also seek applications of the model in engineered multi-agent systems, such as developing control algorithms for robotic teams that use active sensors for navigation.

Chapter 5

Conclusions

5.1 Research summary

Collective formation is generated through assigning various local interaction rules. In Chapter 2, we modeled collective behavior by demanding that individuals align velocity directions with peers that they sense [57]. Collective behavior can also emerge as individuals are attracted to close peers' locations [12]. For the individual interaction rules, researchers have demonstrated that there exists a numerosity constraint on the number of peers for animals to interact with [8]. In many multi-agent animal systems, collective formation also involves leadership and co-leadership which guide the overall group behavior/motion [123, 124]. In addition, a recent study reveals that animals share collective decision making rather than being governed by dominant leaders which adds to the democracy of the multi-agent societies [125]. Therefore, continuous studies can be carried out in regards to studying more accurate mechanisms behind the collective behavior of different animal species.

Predation avoidance strategies among animal collectives can vary due to different animal behaviors and hunting settings. In Chapter 2, the proposed strategies that large cohesive collectives aided predation avoidance resulted from the modeling settings. A change of the modeling perspectives according to real situations may suggest different results. For example, forming large cohesive collectives may not be beneficial if predators are able to follow prey collectives [126]. If predators are not able to consume multiple prey in a time, forming disperse small groups may not be the worst strategy. To propose strategies to avoid hunting or to achieve predation success, the modeling should be customized according to

the considered situations.

The field experiments in Chapter 3 and the simulation in Chapter 4 showed consistency that individual bat increased emissions for more sensory information in collectives. The findings through our field experiments were direct averaging results that showed the increasing biosonar output per bat as swarm size increased. We hypothesized the reason as the necessity for more sensory information, as suggested by the result of the current laboratory findings that bats increased emissions for target detection. The modeling and simulation results directly showed that increasing emissions is beneficial for collision avoidance as individuals obtained more sensory information. Future work of assigning on-board device [104] to individual bats would help verify our findings through both the field experiments and simulation.

5.2 Possible engineering applications

Studying multi-agent animal systems could inspire novel control algorithms for engineered robotic teams [127, 128, 129]. For example, a group of robots could exhibit collective formation as we prescribe alignment and attraction rules to each agent [130, 131, 132]. A robotic team could have better success on detecting multiple objects/prey as we propose appropriate predation strategies inspired by animal hunting. Appropriate increase of individual sensing could help collision avoidance in robotic teams while reducing destructive frequency jamming risk. In addition, studying collective active sensing could help realize the next-generation manned air traffic equipped with active sensing and decentralized control [133]. Last but not the least, we could investigate the collective coordination in task achievement in animal swarms, such as collective transportation by ant colonies, to inspire multi-robot coordination algorithms for achieving engineering tasks [134].

References

[1] Shoham, Y., and Leyton-Brown, K., 2008. *Multiagent systems: Algorithmic, game-theoretic, and logical foundations*. Cambridge University Press.

[2] Li, H., Popa, A., Thibault, C., Trentini, M., and Seto, M., 2010. "A software framework for multi-agent control of multiple autonomous underwater vehicles for underwater mine counter-measures". In IEEE International Conference on Autonomous and Intelligent Systems, pp. 1–6.

[3] Zhuo, W., and Xiao-ning, F., 2011. "A cooperative simulation system for AUV based on multi-agent". In International Conference on Virtual Reality and Visualization, pp. 109–114.

[4] Gorodetski, V., and Kotenko, I., 2002. "The multi-agent systems for computer network security assurance: frameworks and case studies". In 2002 IEEE International Conference on Artificial Intelligence Systems, IEEE, pp. 297–302.

[5] Dasgupta, P., and Das, R., 2000. "Dynamic pricing with limited competitor information in a multi-agent economy". In Cooperative Information Systems, Springer, pp. 299–310.

[6] DeLellis, P., Polverino, G., Ustuner, G., Abaid, N., Macrì, S., Bollt, E. M., and Porfiri, M., 2014. "Collective behaviour across animal species". *Scientific Reports*, **4**.

[7] Abaid, N., and Porfiri, M., 2010. "Fish in a ring: spatio-temporal pattern formation in one-dimensional animal groups". *Journal of the Royal Society Interface*, **7**(51), pp. 1441–1453.

[8] Ballerini, M., Cabibbo, N., Candelier, R., Cavagna, A., Cisbani, E., Giardina, I., Lecomte, V., Orlandi, A., Parisi, G., Procaccini, A., Viale, M., and Zdravkovic, V.,

2008. "Interaction ruling animal collective behavior depends on topological rather than metric distance: Evidence from a field study". *Proceedings of the National Academy of Sciences,* **105**(4), pp. 1232–1237.

[9] Couzin, I. D., and Franks, N. R., 2003. "Self-organized lane formation and optimized traffic flow in army ants". *Proceedings of the Royal Society of London. Series B: Biological Sciences,* **270**(1511), pp. 139–146.

[10] Theriault, D., Wu, Z., Hristov, N., Swartz, S., Breuer, K., Kunz, T., and Betke, M., 2010. Reconstruction and analysis of 3D trajectories of Brazilian free-tailed bats in flight. Tech. rep., Boston University.

[11] Sumpter, D. J., 2006. "The principles of collective animal behaviour". *Philosophical Transactions of the Royal Society B: Biological Sciences,* **361**(1465), pp. 5–22.

[12] Aoki, I., 1982. "A simulation study on the schooling mechanism in fish". *Bulletin of the Japanese Society of Scientific Fisheries,* **48**(8), pp. 1081–1088.

[13] Couzin, I. D., Krause, J., James, R., Ruxton, G. D., and Franks, N. R., 2002. "Collective memory and spatial sorting in animal groups". *Journal of Theoretical Biology,* **218**(1), pp. 1–11.

[14] Lima, S. L., 1995. "Collective detection of predatory attack by social foragers: fraught with ambiguity?". *Animal Behaviour,* **50**(4), pp. 1097–1108.

[15] Roberts, G., 1996. "Why individual vigilance declines as group size increases". *Animal Behaviour,* **51**(5), pp. 1077–1086.

[16] Karsai, I., and Wenzel, J. W., 1998. "Productivity, individual-level and colony-level flexibility, and organization of work as consequences of colony size". *Proceedings of the National Academy of Sciences,* **95**(15), pp. 8665–8669.

[17] Penning, P., Parsons, A., Newman, J., Orr, R., and Harvey, A., 1993. "The effects of group size on grazing time in sheep". *Applied Animal Behaviour Science,* **37**(2), pp. 101–109.

[18] Simmons, J. A., and Vernon, J. A., 1971. "Echolocation: discrimination of targets by the bat, *Eptesicus fuscus*". *Journal of Experimental Zoology,* **176**(3), pp. 315–328.

[19] Simmons, J. A., Fenton, M. B., and Farrell, M. J. O., 1979. "Echolocation and pursuit of prey by bats". *Science,* **203**(4375), pp. 16–21.

[20] Kreucher, C., Kastella, K., and Hero III, A. O., 2005. "Sensor management using an active sensing approach". *Signal Processing,* **85**(3), pp. 607–624.

[21] Musiani, D., Lin, K., and Rosing, T. S., 2007. "Active sensing platform for wireless structural health monitoring". In International Conference on Information Processing in Sensor Networks, pp. 390–399.

[22] Ihn, J. B., and Chang, F. K., 2008. "Pitch-catch active sensing methods in structural health monitoring for aircraft structures". *Structural Health Monitoring,* **7**(1), pp. 5–19.

[23] Barclay, R. M., 1982. "Interindividual use of echolocation calls: eavesdropping by bats". *Behavioral Ecology and Sociobiology,* **10**(4), pp. 271–275.

[24] Chiu, C., Xian, W., and Moss, C. F., 2008. "Flying in silence: echolocating bats cease vocalizing to avoid sonar jamming". *Proceedings of the National Academy of Sciences,* **105**(35), pp. 13116–13121.

[25] Yang, P., Freeman, R. A., and Lynch, K. M., 2007. "Distributed cooperative active sensing using consensus filters". In IEEE International Conference on Robotics and Automation, IEEE, pp. 405–410.

[26] Gillam, E. H., Ulanovsky, N., and McCracken, G. F., 2007. "Rapid jamming avoidance in biosonar". *Proceedings of the Royal Society B: Biological Sciences,* **274**(1610), pp. 651–660.

[27] Hiryu, S., Bates, M. E., Simmons, J. A., and Riquimaroux, H., 2010. "FM echolocating bats shift frequencies to avoid broadcast-echo ambiguity in clutter". *Proceedings of the National Academy of Sciences,* **107**(15), pp. 7048–7053.

[28] Bates, M. E., Stamper, S. A., and Simmons, J. A., 2008. "Jamming avoidance response of big brown bats in target detection". *Journal of Experimental Biology,* **211**(1), pp. 106–113.

[29] Lin, Y., and Abaid, N., 2013. "Collective behavior and predation success in a predator-prey model inspired by hunting bats". *Physical Review E,* **88**(6), p. 062724.

[30] Lin, Y., and Abaid, N., 2013. "Bats versus bugs: Collective behavior of prey decreases predation in a biologically-inspired multi-agent system". In ASME 2013 Dynamic Systems and Control Conference, American Society of Mechanical Engineers, pp. V001T07A002–V001T07A002.

[31] Lin, Y., Nicole, A. T., and Müller, R. "Bats adjust pulse emission behavior with swarm size in the field". *To be submitted*.

[32] Lin, Y., and Abaid, N., 2015. "Modeling perspectives on echolocation strategies inspired by bats flying in groups". *Journal of Theoretical Biology,* **387**, pp. 46–53.

[33] Lin, Y., and Abaid, N., 2014. "Information sharing via active sensing in a multi-agent system inspired by echolocating bats". In ASME 2014 Dynamic Systems and Control Conference, American Society of Mechanical Engineers, pp. V001T05A002–V001T05A002.

[34] Butail, S., Manoukis, N. C., Diallo, M., Ribeiro, J. M. C., and Paley, D. A., 2013. "The dance of male anopheles gambiae in wild mating swarms". *Journal of Medical Entomology,* **50**(3), May, pp. 552–559.

[35] Pitcher, T., Magurran, A., and Winfield, I., 1982. "Fish in larger shoals find food faster". *Behavioral Ecology and Sociobiology,* **10**(2), pp. 149–151.

[36] Trune, D. R., and Slobodchikoff, C. N., 1976. "Social effects of roosting on the metabolism of the pallid bat (*Antrozous pallidus*)". *Journal of Mammalogy,* **57**(4), pp. 656–663.

[37] Cowan, D. P., 1987. "Group living in the european rabbit (*Oryctolagus cuniculus*): Mutual benefit or resource localization?". *Journal of Animal Ecology,* **56**(3), pp. 779–795.

[38] Ioannou, C. C., Guttal, V., and Couzin, I. D., 2012. "Predatory fish select for coordinated collective motion in virtual prey". *Science,* **337**(6099), pp. 1212–1215.

[39] Krause, J., and Ruxton, G. D., 2002. *Living in Groups*. Oxford University Press, Oxford, U.K.

[40] Czirók, A., and Vicsek, T., 2000. "Collective behavior of interacting self-propelled particles". *Physica A: Statistical Mechanics and its Applications,* **281**(1), pp. 17–29.

[41] Toner, J., and Tu, Y., 1998. "Flocks, herds, and schools: A quantitative theory of flocking". *Physical Review E,* **58**(4), pp. 4828–4858.

[42] Czirók, A., Barabási, A.-L., and Vicsek, T., 1999. "Collective motion of self-propelled particles: Kinetic phase transition in one dimension". *Physical Review Letters*, **82**(1), pp. 209–212.

[43] Bonabeau, E., 2002. "Agent-based modeling: Methods and techniques for simulating human systems". *Proceedings of the National Academy of Sciences of the United States of America,* **99**(Suppl 3), May, pp. 7280–7287.

[44] Couzin, I., 2007. "Collective minds". *Nature,* **445**(7129), pp. 715–715.

[45] Cambu, D. S., and Rosas, A., 2012. "Density induced transition in a school of fish". *Physica A: Statistical Mechanics and its Applications,* **391**(15), pp. 3908–3914.

[46] Aureli, M., and Porfiri, M., 2010. "Coordination of self-propelled particles through external leadership". *EPL (Europhysics Letters),* **92**(4), pp. 40004–.

[47] Erdmann, U., Ebeling, W., and Mikhailov, A. S., 2005. "Noise-induced transition from translational to rotational motion of swarms". *Physical Review E,* **71**(5), p. 051904.

[48] Strefler, J., Erdmann, U., and Schimansky-Geier, L., 2008. "Swarming in three dimensions". *Physical Review E,* **78**(3), p. 031927.

[49] Caratozzolo, M., Carnazza, S., Fortuna, L., Frasca, M., Guglielmino, S., Gurrieri, G., and Marletta, G., 2008. "Self-organizing models of bacterial aggregation states". *Mathematical Biosciences and Engineering,* **5**(1), pp. 75–83.

[50] Wang, X., He, M., and Kang, Y., 2012. "A computational predator-prey model, pursuit-evasion behavior based on different range of vision". *Physica A: Statistical Mechanics and its Applications,* **391**(3), pp. 664–672.

[51] Droz, M., and Pekalski, A., 2001. "Coexistence in a predator-prey system". *Physical Review E,* **63**(5), p. 051909.

[52] Simmons, J. A., Ferragamo, M. J., and Moss, C. F., 1998. "Echo-delay resolution in sonar images of the big brown bat, *Eptesicus fuscus*". *Proceedings of the National Academy of Sciences,* **95**(21), pp. 12647–12652.

[53] Hutson, A. M., Mickleburgh, S. P., and Racey, P. A., 2001. *Microchiropteran Bats: Global Status Survey and Conservation Action Plan*, Vol. 56. IUCN, Gland, Switzerland and Cambridge, UK.

[54] Dechmann, D. K., and Safi, K., 2005. "Studying communication in bats". *Cognition, Brain, Behavior,* **9**(3), pp. 479–496.

[55] Surlykke, A., Pedersen, S. B., and Jakobsen, L., 2009. "Echolocating bats emit a highly directional sonar sound beam in the field". *Proceedings of the Royal Society B: Biological Sciences,* **276**(1658), pp. 853–860.

[56] Jakobsen, L., and Surlykke, A., 2010. "Vespertilionid bats control the width of their biosonar sound beam dynamically during prey pursuit". *Proceedings of the National Academy of Sciences,* **107**(31), pp. 13930–13935.

[57] Vicsek, T., Czirók, A., Ben-Jacob, E., Cohen, I., and Shochet, O., 1995. "Novel type of phase transition in a system of self-driven particles". *Physical Review Letters,* **75**(6), pp. 1226–1229.

[58] Grimmett, G., and Stirzaker, D., 2001. *Probability and Random Processes*. Oxford University Press.

[59] Ghose, K., and Moss, C. F., 2003. "The sonar beam pattern of a flying bat as it tracks tethered insects". *The Journal of the Acoustical Society of America,* **114**(2), pp. 1120–1131.

[60] Kerth, G., Wagner, M., and Knig, B., 2001. "Roosting together, foraging apart: information transfer about food is unlikely to explain sociality in female bechstein's bats (*Myotis bechsteinii*)". *Behavioral Ecology and Sociobiology,* **50**(3), pp. 283–291.

[61] Chaté, H., Ginelli, F., Grégoire, G., Peruani, F., and Raynaud, F., 2008. "Modeling collective motion: variations on the Vicsek model". *The European Physical Journal B-Condensed Matter and Complex Systems,* **64**(3), pp. 451–456.

[62] Abaid, N., Bollt, E., and Porfiri, M., 2012. "Topological analysis of complexity in multiagent systems". *Physical Review E,* **85**(4), p. 041907.

[63] Goldman, L., and Henson Jr, O., 1977. "Prey recognition and selection by the constant frequency bat, pteronotus p. parnellii". *Behavioral Ecology and Sociobiology,* **2**(4), pp. 411–419.

[64] Kolpas, A., Moehlis, J., and Kevrekidis, I. G., 2007. "Coarse-grained analysis of stochasticity-induced switching between collective motion states". *Proceedings of the National Academy of Sciences of the United States of America,* **104**(14), pp. 5931–5935.

[65] Aureli, M., Fiorilli, F., and Porfiri, M., 2012. "Portraits of self-organization in fish schools interacting with robots". *Physica D: Nonlinear Phenomena,* **241**(9), pp. 908–920.

[66] Chaté, H., Ginelli, F., Grégoire, G., and Raynaud, F., 2008. "Collective motion of self-propelled particles interacting without cohesion". *Physical Review E,* **77**(4), p. 046113.

[67] Stirzaker, D., 1994. *Elementary Probability*. Cambridge University Press.

[68] Kick, S. A., 1982. "Target-detection by the echolocating bat, *Eptesicus fuscus*". *Journal of Comparative Physiology A: Neuroethology, Sensory, Neural, and Behavioral Physiology,* **145**(4), pp. 431–435.

[69] Au, W. W., and Simmons, J. A., 2007. "Echolocation in dolphins and bats". *Physics Today,* **60**(9), pp. 40–45.

[70] Tian, X., Iriarte-Diaz, J., Middleton, K., Galvao, R., Israeli, E., Roemer, A., Sullivan, A., Song, A., Swartz, S., and Breuer, K., 2006. "Direct measurements of the kinematics and dynamics of bat flight". *Bioinspiration & Biomimetics,* **1**(4), pp. S10–S18.

[71] Rayner, J., and Aldridge, H., 1985. "Three-dimensional reconstruction of animal flight paths and the turning flight of microchiropteran bats". *Journal of Experimental Biology,* **118**(1), pp. 247–265.

[72] Witte, R. S., and Witte, J. S., 2007. *Statistics*. Wiley, Hoboken, N.J.

[73] Schaik, C. P. V., 1983. "Why are diurnal primates living in groups?". *Behaviour,* **87**(1/2), pp. 120–144.

[74] Lima, S. L., and Dill, L. M., 1990. "Behavioral decisions made under the risk of predation: a review and prospectus". *Canadian Journal of Zoology,* **68**(4), pp. 619–640.

[75] Ordemann, A., Balazsi, G., and Moss, F., 2003. "Pattern formation and stochastic motion of the zooplankton *Daphnia* in a light field". *Physica A: Statistical Mechanics and its Applications,* **325**(1), pp. 260–266.

[76] Sugawara, K., and Sano, M., 1997. "Cooperative acceleration of task performance: Foraging behavior of interacting multi-robots system". *Physica D: Nonlinear Phenomena,* **100**(3), pp. 343–354.

[77] Cepeda-Gomez, R., Olgac, N., and Sierra, D. A., 2011. "Application of sliding mode control to swarms under conflict". *IET control theory & applications*, **5**(10), pp. 1167–1175.

[78] Sierra, D. A., McCullough, P., Olgac, N., and Adams, E., 2012. "Control of antagonistic swarm dynamics via lyapunov's method". *Asian Journal of Control*, **14**(1), Jan., pp. 23–35.

[79] Wiggins, D. A., 1991. "Foraging success and aggression in solitary and group-feeding great egrets (casmerodius albus)". *Colonial Waterbirds*, **14**, pp. 176–179.

[80] Packer, C., Scheel, D., and Pusey, A. E., 1990. "Why lions form groups: food is not enough". *The American Naturalist*, **136**, pp. 1–19.

[81] Fritz, H., and De Garine-Wichatitsky, M., 1996. "Foraging in a social antelope: effects of group size on foraging choices and resource perception in impala". *Journal of Animal Ecology*, **65**, pp. 736–742.

[82] Bednekoff, P. A., and Lima, S. L., 1998. "Reexamining safety in numbers: interactions between risk dilution and collective detection depend upon predator targeting behaviour". *Proceedings of the Royal Society of London. Series B: Biological Sciences*, **265**(1409), pp. 2021–2026.

[83] Polverino, G., and Porfiri, M., 2013. "Zebrafish (*Danio rerio*) behavioural response to bioinspired robotic fish and mosquitofish (*Gambusia affinis*)". *Bioinspiration & Biomimetics*, **8**(4), pp. 044001–044007.

[84] Jadaliha, M., and Choi, J., 2013. "Environmental monitoring using autonomous aquatic robots: Sampling algorithms and experiments". *IEEE Transactions on Control Systems Technology*, **21**(3), pp. 899–905.

[85] Spinello, D., and Stilwell, D. J., 2011. "Formation control of platoons of mobile sensors with intermittent communications". In ASME 2011 Dynamic Systems and Control Conference, Vol. 1, ASME, Arlington VA, pp. 25–32.

[86] Müller, R., 2010. "Numerical analysis of biosonar beamforming mechanisms and strategies in bats". *The Journal of the Acoustical Society of America*, **128**(3), pp. 1414–1425.

[87] Betke, M., Hirsh, D. E., Makris, N. C., McCracken, G. F., Procopio, M., Hristov, N. I., Tang, S., Bagchi, A., Reichard, J. D., and Horn, J. W., 2008. "Thermal imaging reveals significantly smaller Brazilian free-tailed bat colonies than previously estimated". *Journal of Mammalogy*, **89**(1), pp. 18–24.

[88] Hristov, N. I., Betke, M., Theriault, D. E., Bagchi, A., and Kunz, T. H., 2010. "Seasonal variation in colony size of Brazilian free-tailed bats at Carlsbad Cavern based on thermal imaging". *Journal Information,* **91**(1).

[89] Zahn, A., 1999. "Reproductive success, colony size and roost temperature in attic-dwelling bat *Myotis*". *Journal of Zoology,* **247**(2), pp. 275–280.

[90] Betke, M., Hirsh, D. E., Bagchi, A., Hristov, N. I., Makris, N. C., and Kunz, T. H., 2007. "Tracking large variable numbers of objects in clutter". In IEEE Conference on Computer Vision and Pattern Recognition, pp. 1–8.

[91] Simmons, J. A., 1989. "A view of the world through the bat's ear: the formation of acoustic images in echolocation". *Cognition,* **33**(1), pp. 155–199.

[92] Yan, J., and Suga, N., 1996. "The midbrain creates and the thalamus sharpens echo-delay tuning for the cortical representation of target-distance information in the mustached bat". *Hearing research,* **93**(1), pp. 102–110.

[93] Wotton, J., and Simmons, J., 2000. "Spectral cues and perception of the vertical position of targets by the big brown bat, *Eptesicus fuscus*". *The Journal of the Acoustical Society of America,* **107**(2), pp. 1034–1041.

[94] Simmons, J. A., Ferragamo, M., Moss, C. F., Stevenson, S. B., and Altes, R. A., 1990. "Discrimination of jittered sonar echoes by the echolocating bat, *Eptesicus fuscus*: the shape of target images in echolocation". *Journal of Comparative Physiology A,* **167**(5), pp. 589–616.

[95] Simmons, J. A., Moss, C. F., and Ferragamo, M., 1990. "Convergence of temporal and spectral information into acoustic images of complex sonar targets perceived by the echolocating bat, *Eptesicus fuscus*". *Journal of Comparative Physiology A,* **166**(4), pp. 449–470.

[96] Ulanovsky, N., Fenton, M. B., Tsoar, A., and Korine, C., 2004. "Dynamics of jamming avoidance in echolocating bats". *Proceedings of the Royal Society of London. Series B: Biological Sciences,* **271**(1547), pp. 1467–1475.

[97] Jarvis, J., Jackson, W., and Smotherman, M., 2013. "Groups of bats improve sonar efficiency through mutual suppression of pulse emissions". *Frontiers in Physiology,* **4**(140), pp. 1–9.

[98] Hiryu, S., Katsura, K., Nagato, T., Yamazaki, H., Lin, L.-K., Watanabe, Y., and Riquimaroux, H., 2006. "Intra-individual variation in the vocalized frequency of the taiwanese leaf-nosed bat, *Hipposideros terasensis*, influenced by conspecific colony members". *Journal of Comparative Physiology A,* **192**(8), pp. 807–815.

[99] Gillam, E. H., Hristov, N. I., Kunz, T. H., and McCracken, G. F., 2010. "Echolocation behavior of Brazilian free-tailed bats during dense emergence flights". *Journal of Mammalogy,* **91**(4), pp. 967–975.

[100] Hristov, N. I., Allen, L. C., and Chadwell, B. A., 2013. "New advances in the study of group behavior in bats". In *Bat Evolution, Ecology, and Conservation*. Springer, pp. 271–291.

[101] Thabah, A., Li, G., Wang, Y., Liang, B., Hu, K., Zhang, S., and Jones, G., 2007. "Diet, echolocation calls, and phylogenetic affinities of the great evening bat (*Ia io; Vespertilionidae*): another carnivorous bat". *Journal of Mammalogy,* **88**(3), pp. 728–735.

[102] Russoa, D., and Papadatou, E., 2014. "Acoustic identification of free-flying schreiber's bat *Miniopterus schreibersii* by social calls". *Hysterix,* **25**(2), pp. 119–120.

[103] Ratcliffe, J. M., Elemans, C. P. H., Jakobsen, L., and Surlykke, A., 2013. "How the bat got its buzz". *Biology Letters,* **9**(2).

[104] Cvikel, N., Levin, E., Hurme, E., Borissov, I., Boonman, A., Amichai, E., and Yovel, Y., 2015. "On-board recordings reveal no jamming avoidance in wild bats". *Proceedings of the Royal Society of London B: Biological Sciences,* **282**(1798), p. 20142274.

[105] Liu, M., and Müller, R., in prep.. "Evaluation of a simple model for the acoustics of bat swarms". *The Journal of the Acoustical Society of America*.

[106] Funakoshi, K., Arai, A., and Inoue, T., 2013. "Development of sounds during postnatal growth of the eastern bent-winged bat *Miniopterus fuliginosus*". *Mammal study,* **38**(1), pp. 49–56.

[107] DiCecco, J., Gaudette, J. E., and Simmons, J. A., 2013. "Multi-component separation and analysis of bat echolocation calls". *The Journal of the Acoustical Society of America,* **133**(1), pp. 538–546.

[108] Gao, L., Balakrishnan, S., He, W., Yan, Z., and Müller, R., 2011. "Ear deformations give bats a physical mechanism for fast adaptation of ultrasonic beam patterns". *Physical Review Letters*, **107**(21), p. 214301.

[109] Horowitz, S. S., Cheney, C. A., and Simmons, J. A., 2004. "Interaction of vestibular, echolocation, and visual modalities guiding flight by the big brown bat, *Eptesicus fuscus*". *Journal of Vestibular Research*, **14**(1), pp. 17–32.

[110] Bates, M. E., Simmons, J. A., and Zorikov, T. V., 2011. "Bats use echo harmonic structure to distinguish their targets from background clutter". *Science*, **333**(6042), pp. 627–630.

[111] Kashima, K., Ohtsuki, H., and Satake, A., 2013. "Fission-fusion bat behavior as a strategy for balancing the conflicting needs of maximizing information accuracy and minimizing infection risk". *Journal of Theoretical Biology*, **318**, pp. 101–109.

[112] Corcoran, A. J., and Conner, W. E., 2014. "Bats jamming bats: Food competition through sonar interference". *Science*, **346**(6210), pp. 745–747.

[113] Lopez, U., Gautrais, J., Couzin, I. D., and Theraulaz, G., 2012. "From behavioural analyses to models of collective motion in fish schools". *Interface Focus*, p. 20120033.

[114] Olson, R. S., Hintze, A., Dyer, F. C., Knoester, D. B., and Adami, C., 2013. "Predator confusion is sufficient to evolve swarming behaviour". *Journal of The Royal Society Interface*, **10**(85), p. 20130305.

[115] Angelani, L., 2012. "Collective predation and escape strategies". *Physical Review Letters*, **109**(11), p. 118104.

[116] Wynn, M. L., Kulesa, P. M., and Schnell, S., 2012. "Computational modelling of cell chain migration reveals mechanisms that sustain follow-the-leader behaviour". *Journal of The Royal Society Interface*, **9**(72), pp. 1576–1588.

[117] Jiang, W., Sullivan, A. M., Su, C., and Zhao, X., 2012. "An agent-based model for the transmission dynamics of *Toxoplasma gondii*". *Journal of Theoretical Biology*, **293**, pp. 15–26.

[118] Tully, S., Cojocaru, M., and Bauch, C. T., 2013. "Coevolution of risk perception, sexual behaviour, and HIV transmission in an agent-based model". *Journal of Theoretical Biology*, **337**, pp. 125–132.

[119] Speakman, J., and Racey, P., 1991. "No cost of echolocation for bats in flight". *Nature,* **350**(6317), pp. 421–423.

[120] Salehipour, H., and Willis, D. J., 2013. "A coupled kinematics-energetics model for predicting energy efficient flapping flight". *Journal of Theoretical Biology,* **318**, pp. 173–196.

[121] Agosta, S. J., 2002. "Habitat use, diet and roost selection by the big brown bat (*Eptesicus fuscus*) in North America: a case for conserving an abundant species". *Mammal Review,* **32**(3), pp. 179–198.

[122] Hamilton, I. M., and Barclay, R. M., 1998. "Ontogenetic influences on foraging and mass accumulation by big brown bats (*Eptesicus fuscus*)". *Journal of Animal Ecology,* **67**(6), pp. 930–940.

[123] Nagy, M., Ákos, Z., Biro, D., and Vicsek, T., 2010. "Hierarchical group dynamics in pigeon flocks". *Nature,* **464**(7290), pp. 890–893.

[124] Krause, J., Hoare, D., Krause, S., Hemelrijk, C., and Rubenstein, D., 2000. "Leadership in fish shoals". *Fish and Fisheries,* **1**(1), pp. 82–89.

[125] Strandburg-Peshkin, A., Farine, D. R., Couzin, I. D., and Crofoot, M. C., 2015. "Shared decision-making drives collective movement in wild baboons". *Science,* **348**(6241), pp. 1358–1361.

[126] Major, P. F., 1978. "Predator-prey interactions in two schooling fishes, caranx ignobilis and stolephorus purpureus". *Animal Behaviour,* **26**, pp. 760–777.

[127] Kube, C. R., and Zhang, H., 1993. "Collective robotics: From social insects to robots". *Adaptive behavior,* **2**(2), pp. 189–218.

[128] Parker, L. E., 2000. "Current state of the art in distributed autonomous mobile robotics". In *Distributed Autonomous Robotic Systems 4*. Springer, pp. 3–12.

[129] Şahin, E., 2005. "Swarm robotics: From sources of inspiration to domains of application". In *Swarm robotics*. Springer, pp. 10–20.

[130] Hsieh, M. A., Halász, Á., Berman, S., and Kumar, V., 2008. "Biologically inspired redistribution of a swarm of robots among multiple sites". *Swarm Intelligence,* **2**(2-4), pp. 121–141.

[131] Berman, S., Halász, Á., Kumar, V., and Pratt, S., 2007. "Algorithms for the analysis and synthesis of a bio-inspired swarm robotic system". In *Swarm Robotics*. Springer, pp. 56–70.

[132] Berman, S., Lindsey, Q., Sakar, M. S., Kumar, V., and Pratt, S. C., 2011. "Experimental study and modeling of group retrieval in ants as an approach to collective transport in swarm robotic systems". *Proceedings of the IEEE,* **99**(9), pp. 1470–1481.

[133] Romli, F., King, J., Li, L., and Clarke, J.-P., 2008. "Impact of automatic dependent surveillance-broadcast (ADS-B) on traffic alert and collision avoidance system (TCAS) performance". In AIAA Guidance, Navigation, and Control Conference and Exhibit, AIAA, p. 6971.

[134] Werfel, J., Petersen, K., and Nagpal, R., 2014. "Designing collective behavior in a termite-inspired robot construction team". *Science,* **343**(6172), pp. 754–758.

Appendix - Journal copyright permissions

Chapter 2 is the paper published in Physical Review E [29] which belongs to American Physical Society (APS). According to the copyright policy from APS, "the author has the right to use the article or a portion of the article in a thesis or dissertation without requesting permission from APS, provided the bibliographic citation and the APS copyright credit line are given on the appropriate pages." Thus, the permission to include the paper as Chapter 2 is granted. Detailed information about APS copyright information can be found through this link: https://journals.aps.org/copyrightFAQ.html#thesis. The paper can be found through this link: http://journals.aps.org/pre/abstract/10.1103/PhysRevE.88.062724.

Chapter 4 is the paper published in the Journal of Theoretical Biology [32] which belongs to Elsevier. According to the copyright policy from Elsevier, the authors can include the articles in a thesis or dissertation provided that this is not to be published commercially. Thus, the permission to include the paper as Chapter 4 is granted. Detailed information about Elsevier copyright information can be found through this link: https://www.elsevier.com/about/company-information/policies/copyright. The paper can be searched here: http://www.sciencedirect.com/science/article/pii/S0022519315004427.